Article

Cell

A Receptor Pair with an Integrated Decoy Converts Pathogen Disabling of Transcription Factors to Immunity

Graphical Abstract

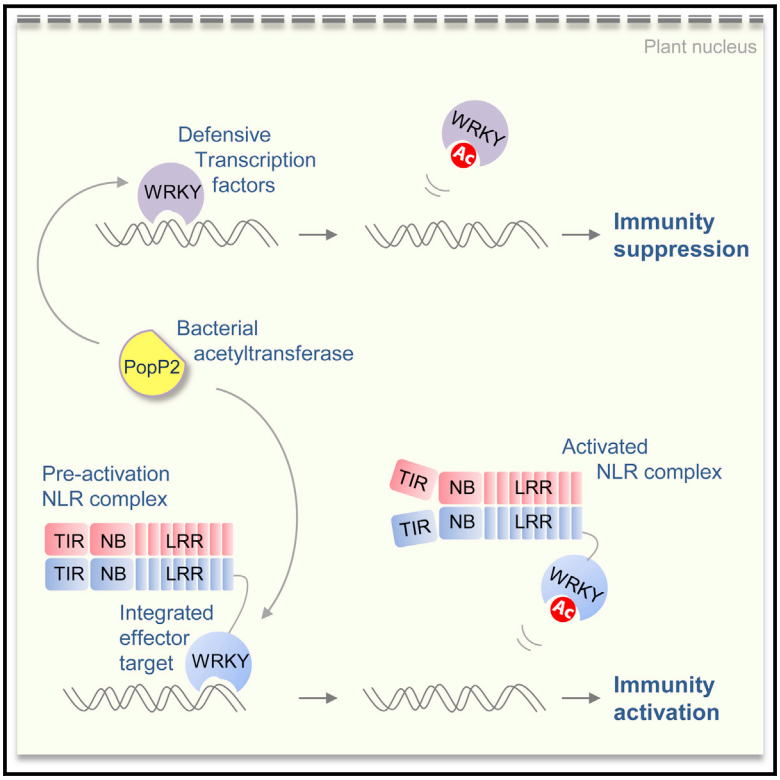

Highlights

- A bacterial lysine acetyltransferase targets multiple plant transcription factors
- Target acetylation disables transcription-factor-DNA binding and host immunity
- Immune receptor RRS1-R uses the same DNA-binding domain as an effector bait
- Effector acetylation of RRS1-R converts disease susceptibility into robust defense

Authors

Clémentine Le Roux, Gaëlle Huet, ..., Jane E. Parker, Laurent Deslandes

Correspondence

laurent.deslandes@toulouse.inra.fr

In Brief

A plant immune receptor pair effectively intercepts pathogen-mediated disabling of a large family of defensive transcription factors at the DNA level by incorporating a transcriptional decoy domain to trigger activation of the receptor complex and immunity.

Le Roux et al., 2015, Cell *161*, 1074–1088
May 21, 2015
http://dx.doi.org/10.1016/j.cell.2015.04.025

CellPress

Cell

Article

A Receptor Pair with an Integrated Decoy Converts Pathogen Disabling of Transcription Factors to Immunity

Clémentine Le Roux,[1,2,3,11] Gaëlle Huet,[1,2,11] Alain Jauneau,[4] Laurent Camborde,[5,6] Dominique Trémousaygue,[1,2] Alexandra Kraut,[7,8,9] Binbin Zhou,[1,2] Marie Levaillant,[1,2] Hiroaki Adachi,[10] Hirofumi Yoshioka,[10] Sylvain Raffaele,[1,2] Richard Berthomé,[1,2] Yohann Couté,[7,8,9] Jane E. Parker,[3] and Laurent Deslandes[1,2,*]

[1]INRA, Laboratoire des Interactions Plantes-Microorganismes (LIPM), UMR441, Castanet-Tolosan 31326, France
[2]CNRS, Laboratoire des Interactions Plantes-Microorganismes (LIPM), UMR2594, Castanet-Tolosan 31326, France
[3]Department of Plant-Microbe Interactions, Max Planck Institute for Plant Breeding Research, Carl-von-Linne-Weg 10, Köln 50829, Germany
[4]Institut Fédératif de Recherche 3450, Plateforme Imagerie, Pôle de Biotechnologie Végétale, Castanet-Tolosan 31326, France
[5]Laboratoire de Recherche en Sciences Végétales, Université de Toulouse, UPS, UMR 5546, BP 42617 Auzeville, Castanet-Tolosan 31326, France
[6]CNRS, UMR 5546, BP 42617, Castanet-Tolosan 31326, France
[7]Université Grenoble Alpes, iRTSV-BGE, Grenoble 38000, France
[8]CEA, iRTSV-BGE, Grenoble 38000, France
[9]INSERM, BGE, Grenoble 38000, France
[10]Defense in Plant-Pathogen Interactions, Graduate School of Bioagricultural Sciences, Nagoya University, Chikusa, Nagoya 464-8601, Japan
[11]Co-first author
*Correspondence: laurent.deslandes@toulouse.inra.fr
http://dx.doi.org/10.1016/j.cell.2015.04.025

SUMMARY

Microbial pathogens infect host cells by delivering virulence factors (effectors) that interfere with defenses. In plants, intracellular nucleotide-binding/leucine-rich repeat receptors (NLRs) detect specific effector interference and trigger immunity by an unknown mechanism. The *Arabidopsis*-interacting NLR pair, RRS1-R with RPS4, confers resistance to different pathogens, including *Ralstonia solanacearum* bacteria expressing the acetyltransferase effector PopP2. We show that PopP2 directly acetylates a key lysine within an additional C-terminal WRKY transcription factor domain of RRS1-R that binds DNA. This disrupts RRS1-R DNA association and activates RPS4-dependent immunity. PopP2 uses the same lysine acetylation strategy to target multiple defense-promoting WRKY transcription factors, causing loss of WRKY-DNA binding and transactivating functions needed for defense gene expression and disease resistance. Thus, RRS1-R integrates an effector target with an NLR complex at the DNA to switch a potent bacterial virulence activity into defense gene activation.

INTRODUCTION

In plant and animal innate immunity, individual cells express receptors to detect pathogens. Plasma membrane pattern recognition receptors (PRRs) sense conserved pathogen molecules (pathogen-associated molecular patterns; PAMPs) to trigger a first line of resistance known as pattern-triggered immunity (PTI). Further pathogen interference is monitored by intracellular nucleotide-binding/leucine-rich-repeat receptors (NLRs) (Maekawa et al., 2011). Mammalian NLRs intercept intracellular PAMPs or pathogen-modified host molecules (damage-associated molecular patterns; DAMPs) to induce immunity (Maekawa et al., 2011; von Moltke et al., 2013). By contrast, plant NLRs recognize variable, often host-specific, pathogen virulence factors (effectors) that are delivered into host cells to promote infection by dampening PTI basal resistance pathways (Dodds and Rathjen, 2010; Maekawa et al., 2011).

NLRs behave as ligand-dependent ATP/ADP-exchanging molecular switches that undergo a series of conformational changes from auto-inhibited to activated molecules in response to pathogen interference (Griebel et al., 2014; Takken and Goverse, 2012).

Cycles of pathogen effector-triggered susceptibility (ETS) and NLR-mediated effector-triggered immunity (ETI) are major forces shaping plant host-pathogen co-evolution (Jones and Dangl, 2006). ETI involves a rebooting of PTI transcriptional programs and often localized host cell death at infection sites (Jones and Dangl, 2006; Maekawa et al., 2011). In some cases, physical NLR-effector interaction underlies disease resistance specificity (Césari et al., 2014; Kanzaki et al., 2012; Maekawa et al., 2011). Other molecularly characterized NLRs are activated through indirect effector recognition, in which effector interference with a host target (cofactor or bait) is sensed by the NLR, acting as a guard of modified "self" (Dodds and Rathjen, 2010; Maekawa et al., 2011). NLR recognition of diverse effector actions on a limited set of defense hubs might further extend NLR interception space. An effector "decoy" model has been proposed for a number of effector-sensing NLRs, in which the guarded host protein has no defense role but resembles an operational effector target and thus serves as a molecular trap to protect related defense components (Lewis et al., 2013; Ntoukakis

et al., 2014; van der Hoorn and Kamoun, 2008). Certain plant NLRs mediating specific pathogen effector recognition function inside nuclei, and some bind transcription factors (TFs) with roles in defense reprogramming (Chang et al., 2013; Inoue et al., 2013; Padmanabhan et al., 2013), suggesting a short path between receptor activation and downstream signaling in ETI. Nevertheless, the processes by which NLR activation mobilizes defense pathways remain obscure.

Here, we examine ETI conditioned by a co-functioning *Arabidopsis* NLR pair, RRS1-R (RESISTANCE TO RALSTONIA SOLANACEARUM1) and RPS4 (RESISTANCE TO PSEUDOMONAS SYRINGAE4), which belong to an NLR subfamily with N-terminal TIR (Toll-Interleukin1 Receptor) signaling domains (referred to as TNLs) (Griebel et al., 2014). RRS1-R/RPS4 cooperate genetically and molecularly in resistance to different pathogens, including root-infecting *Ralstonia solanacearum* bacteria expressing the type-III secreted effector (T3SE) PopP2, a member of the YopJ superfamily of acetyltransferases (Deslandes et al., 2003; Tasset et al., 2010) and an unrelated T3SE, AvrRps4, from leaf-infecting *Pseudomonas syringae* pathovar *pisi* (Hinsch and Staskawicz, 1996; Sohn et al., 2012). Molecular and structural analyses of RRS1-R/RPS4 interactions suggest that a heterodimer (or oligomer) with juxtaposed TIR domains represents an inhibited, pre-activation receptor complex that is activated by direct binding of PopP2 or AvrRps4 to RRS1-R (Williams et al., 2014). Activation causes heterocomplex rearrangements to initiate signaling (Williams et al., 2014). Thus, RRS1-R functions as both the inhibiting and effector-sensing molecule for this receptor pair.

The extreme C-terminal portion of RRS1-R contains a conserved "WRKY" DNA-binding domain of plant WRKY TFs that orchestrate biotic stress responses by recognizing W-box motifs in gene promoters (Rushton et al., 2010). Because PopP2 interacts with RRS1-R in plant nuclei and PopP2 acetyltransferase activity is necessary to trigger RRS1-R/RPS4 immunity (Tasset et al., 2010), we postulated that RRS1-R recognizes PopP2 activity. In animals, acetyltransferase activities of several YopJ-like effectors disrupt innate immune signaling (Jones et al., 2008; Meinzer et al., 2012). The founding member, YopJ, from *Yersinia pestis* inhibits proinflammatory responses through acetylation of critical serines and threonines in the activation loop of immune-related kinases (Mittal et al., 2006). In plants, *P. syringae* YopJ-like HopZ1a contributes to bacterial infection through acetylation of jasmonate ZIM-domain (JAZ) transcriptional repressors of jasmonic acid signaling (Jiang et al., 2013). We show that PopP2 uses a different virulence strategy to dampen innate immunity by Nε-acetylating a key lysine (Lys) residue within the WRKY domains of numerous WRKY TFs. The Lys modification disables their DNA binding and transcriptional activation of defense genes. PopP2 transacetylase activity on the WRKY domain of RRS1-R switches an inhibited NLR complex into activated NLRs at the chromatin.

RESULTS

PopP2 Causes RRS1-R Acetylation

We tested whether RRS1-R is a PopP2 acetylation substrate. RRS1-R fused to a GFP tag (RRS1-R-GFP) was co-expressed transiently in *N. benthamiana* cells with triple hemagglutinin (HA) epitope-tagged β-glucuronidase (GUS-3HA), PopP2 (PopP2-3HA), or the catalytically inactive PopP2-C321A mutant (C321A-3HA) (Tasset et al., 2010) (Figure 1A). RRS1-R-GFP was purified from protein extracts using a GFP affinity matrix. Immunoblots were probed with anti-HA or anti-GFP antibodies revealing similar amounts of RRS1-R-GFP with co-expressed β-glucuronidase (GUS), PopP2, or C321A. We next probed immunoblots with anti-acetyl-lysine (anti-Ac-K) antibodies to test for RRS1-R-GFP acetylation. Acetylated RRS1-R-GFP (Ac-RRS1-R) was detected with catalytically active PopP2 but not GUS or C321A (Figure 1A). Therefore, PopP2 enzymatic activity causes Nε-acetylation of RRS1-R Lys residues.

To identify the RRS1-R residues modified by PopP2, purified RRS1-R-GFP co-expressed with PopP2 or C321A was used for mass spectrometry-based proteomic analysis in three independent experiments. Coverage of 67% RRS1-R sequence identified two Nε-acetylated Lys residues (Lys-1217 and Lys-1221) with catalytically active PopP2 (Table 1). These two Lys residues reside in the WRKY domain heptad ($WRK^{1217}YGQK^{1221}$), a canonical DNA-binding motif present in all WRKY TFs (Rushton et al., 2010) and at the RRS1-R C terminus (Figure 1B). Lys-1217 was identified in three peptides but was acetylated in only one; by contrast, Lys-1221 was acetylated in all peptides spanning this position (Tables 1 and S1). Therefore, Lys-1221 was the predominant Lys residue modified by PopP2.

PopP2 Directly Acetylates the WRKY Domain of RRS1-R

We confirmed that PopP2 modifies the RRS1-R WRKY domain by co-expressing the 189-amino-acid C-terminal portion of RRS1-R containing the WRKY domain (position 1190–1379, hereinafter called RRS1-R_{Cterm}) fused to GFP with GUS-3HA, PopP2-3HA, or C321A-3HA in *N. benthamiana* (Figure S1A). Immunoblotting with anti-GFP and anti-Ac-K antibodies revealed PopP2-dependent Lys acetylation of immuno-purified RRS1-R_{Cterm}-GFP protein (Figure S1A).

We tested whether RRS1-R is a direct PopP2 substrate. In *Escherichia coli*, expressed PopP2 undergoes auto-acetylation, indicating that the recombinant enzyme is functional (Tasset et al., 2010). Using this bacterial assay, we tested for acetylation of the RRS1-R WRKY domain by PopP2. For this, RRS1-R_{Cterm} was expressed as a fusion with N-terminal glutathione S-transferase (GST) and a C-terminal six-histidine residue (His_6) tag (GST-RRS1-R_{Cterm}-His_6) together with His_6-PopP2 or His_6-C321A. GST-RRS1-R_{Cterm}-His_6 was GST-affinity purified from both extracts. Immunoblot analysis of the GST-purified proteins with anti-His_6 and anti-Ac-K antibodies revealed the presence of acetylated RRS1-R_{Cterm} when co-expressed with PopP2 but not with catalytically inactive C321A (Figure 1C).

Mass spectrometry analysis of the acetylated and non-acetylated immuno-purified RRS1-R_{Cterm}-GFP and GST-RRS1-R_{Cterm}-His_6 forms (expressed in *N. benthamiana* and *E. coli*, respectively) confirmed PopP2-dependent acetylation of RRS1-R at Lys-1221, as observed with full-length RRS1-R protein (Tables 1 and S1). Therefore, Lys-1221 of the RRS1-R C-terminal WRKY domain is directly acetylated by PopP2.

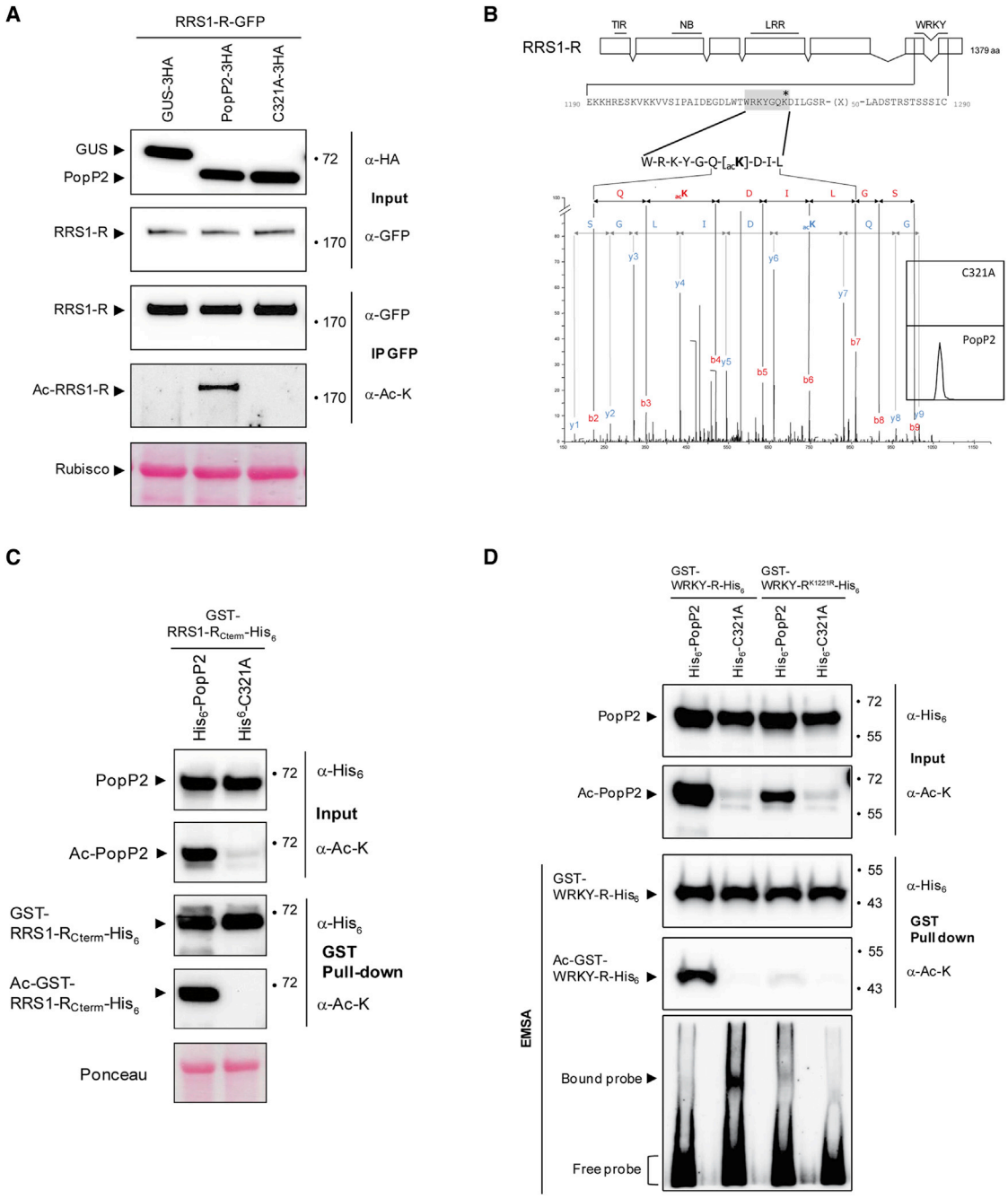

Figure 1. PopP2 Acetylates RRS1-R

(A) RRS1-R-GFP was transiently expressed with 3HA-tagged GUS, PopP2, or C321A in *N. benthamiana* leaves. Protein extracts were immunoblotted with anti-GFP (α-GFP) and anti-HA antibodies (α-HA) (Input). IP was conducted with anti-GFP beads (IP GFP) and analyzed on immunoblots with α-GFP antibodies for detection of RRS1-R or α-acetyl lysine antibodies for detection of acetylated RRS1-R. Results were consistent in three independent experiments.

(B) Representation of the *RRS1-R* gene (seven exons and functional domains). The WRKY heptad domain (gray) is indicated. PopP2-acetylated Lys-1221 is marked by an asterisk. Mass-spectrometry-based proteomic analysis of RRS1-R peptides spanning amino acids 1219–1226 identified acetylated Lys-1221. Peptide GQ[$_{ac}$K^{1221}]DILGS was identified based on matched b- and y-ion series indicated by spectrum annotations. Inset box on right contains extracted chromatograms for the m/z (mass-to-charge ratio) window 589.8 to 589.85 Da from analyses of RRS1-R co-expressed with PopP2 or C321A. Chromatogram x- and y-axis units are equally scaled; x axis is time (minutes), and y-axis units are in relative abundance (0%–100%). Results were consistent in three independent experiments.

(C) PopP2 acetylates RRS1-R$_{Cterm}$ in bacterial cells. GST-RRS1-R$_{Cterm}$-His$_6$ was co-expressed with His$_6$-PopP2 or His$_6$-C321A in *E. coli*. Input indicates protein samples before pull-down. Autoacetylated wild-type PopP2 (Ac-PopP2), but not C321A, is recognized by α-acetyl lysine antibody (Input). GST-purified proteins

(legend continued on next page)

Table 1. Acetyl-Peptides Detected by Tandem Mass Spectrometry Analysis of WRKY Proteins

Protein	Effector	Expressed in	Spectral Counts	Coverage (%)	Acetyl-Peptides	
RRS1-R	PopP2	*N. benth*	309	67	…[acK1217]YGQKDIL…	…KYGQ[acK1221]DIL…
					1/3	11/11
	C321A	*N. benth*	291	64	0/1	0
RRS1-R_{Cterm}	PopP2	*N. benth*	238	61	…[acK1217]YGQKDIL…	…KYGQ[acK1221]DIL…
					5/5	16/16
	C321A	*N. benth*	168	52	0/1	0/2
	PopP2	*E. coli*	303	62	1/9	23/23
	C321A	*E. coli*	213	62	0	0/1
AtWRKY22	PopP2	*N. benth*	130	70	…KYGQ[acK139]PIK…	…KYGQKPI[acK142]GSP…
					9/9	5/9
	C321A	*N. benth*	97	62	1/3	1/3
	PopP2	*E. coli*	138	58	4/4	1/4
	C321A	*E. coli*	126	66	0/2	0/2
AtWRKY30	PopP2	*E. coli*	211	59	…DGFSWR[acK120]…	…YGQ[acK124]DIL…
					1/7	15/16
	C321A	*E. coli*	169	55	0/1	1/2
AtWRKY40	PopP2	*N. benth*	160	84	…[acK63]QLMEY…	…VYY[acK135]TEASDT…
					0/10	1/5
	C321A	*N. benth*	147	77	0/2	0/1
	PopP2	*E. coli*	124	64	1/8	0/4
	C321A	*E. coli*	116	43	0/6	0/2
RRS1-S	PopP2	*N. benth*	448	70	…[acK1215]YGQKDIL…	…KYGQ[acK1219]DIL…
					1/3	12/12
	C321A	*N. benth*	512	68	0/2	0/1
RRS1-S_{Cterm}	PopP2	*E. coli*	283	77	…[acK1215]YGQKDIL…	…KYGQ[acK1219]DIL…
					1/12	26/26
	C321A	*E. coli*	271	66	0/1	0/1

Fluorescent protein-tagged RRS1-R, RRS1-R_{Cterm}, AtWRKY22, AtWRKY40, or RRS1-S was co-expressed with PopP2-3HA or C321A-3HA in *N. benthamiana* (*N. benth*) and purified using GFP beads. GST-tagged RRS1-R_{Cterm}, AtWRKY22, AtWRKY30, AtWRKY40, or RRS1-S_{Cterm} proteins were co-expressed with His_6-PopP2 or His_6-C321A in *Escherichia coli* (*E. coli*) and purified on a GST affinity matrix. Purified proteins were analyzed by liquid chromatography-tandem mass spectrometry (LC-MS/MS), and acetylated Lys residues were identified. Number of total peptides identified in a given round of LC-MS/MS analysis (Spectral counts) and percentage of sequence coverage (Coverage) are indicated. Conserved residues of the WRKYGQK heptad detected in acetylated peptides are underlined. Frequency of detection of acetylated peptides is indicated by fraction numbers.

See also Table S1.

PopP2 Acetylation Disrupts RRS1-R Binding to Genomic DNA

We tested whether RRS1-R WRKY domain acetylation by PopP2 alters RRS1-R DNA-binding activity. For this, we undertook a FRET-FLIM (fluorescence resonance energy transfer-fluorescence lifetime imaging microscopy) approach used to detect protein-DNA associations in animal cells (Cremazy et al., 2005). To monitor RRS1-R binding to DNA in situ, RRS1-R-GFP expressed in *N. benthamiana* (Figure 1A) was used as a FRET donor in combination with Sytox Orange, a DNA-binding fluorescent dye as acceptor. The Sytox Orange absorption spectrum overlaps with the emission spectrum of GFP,

were analyzed by immunoblotting with α-His_6 and α-acetyl lysine antibodies as indicated. Ponceau staining shows protein loading. Results were consistent in at least three independent experiments.

(D) Binding of recombinant acetylated RRS1-R WRKY domain to W-boxes is inhibited in EMSA. GST-WRKY-R-His_6 and GST-WRKY-R^{K1221R}-His_6 were expressed with His_6-PopP2 or His_6-C321A in *E. coli*. Input indicates protein samples before IP. Autoacetylated wild-type PopP2 (Ac-PopP2), but not C321A, is recognized by α-acetyl lysine antibody (Input). GST-fusion proteins were affinity purified and analyzed by immunoblotting with α-His_6 and α-acetyl lysine antibodies as indicated. For EMSA, equal amounts of GST-purified proteins were incubated with a biotin-labeled W-box probe. Purified non-acetylated GST-WRKY-R-His_6 co-expressed with His_6-C321A retained DNA binding as indicated (Bound probe). GST-WRKY-R-His_6 acetylated by His_6-PopP2 and GST-WRKY-R^{K1221R}-His_6 mutant expressed with His_6-PopP2 or His_6-C321A had impaired W-box binding activity. Results were consistent in three independent experiments.

See also Figure S1.

Table 2. FRET-FLIM Measurements Showing that Active PopP2 Inhibits the DNA-Binding Activity of Various WRKY Proteins

Donor	Effector	Acceptor	τ[a]	SE	Δt[b]	n[c]	FRET[d]	p[e]
RRS1-R-GFP	NE	–	2.203	0.030	376	45	17.0	1.4×10^{-11}
		+	1.827	0.038		37		
	PopP2	–	2.272	0.034	27	35	1.2	0.60
		+	2.245	0.037		40		
	C321A	–	2.222	0.035	298	35	13.5	1.5×10^{-8}
		+	1.924	0.031		50		
RRS1-R_{Cterm}-GFP	NE	–	2.175	0.037	272	31	12.5	3.6×10^{-6}
		+	1.903	0.037		31		
	PopP2	–	2.159	0.026	78	40	3.6	0.097
		+	2.081	0.041		30		
	C321A	–	2.135	0.041	237	30	11.1	3×10^{-4}
		+	1.898	0.045		30		
RRS1-R^{K1221R}-GFP	NE	–	2.166	0.066	20	10	0.9	0.79
		+	2.146	0.041		15		
RRS1-R^{K1221Q}-GFP	NE	–	2.201	0.035	−32	32	-	0.65
		+	2.233	0.065		29		
RRS1-R^{SLH1}-GFP	NE	–	2.147	0.038	−8	31	-	0.86
		+	2.155	0.031		30		
AtWRKY22-GFP	NE	–	2.154	0.042	382	30	17.0	7×10^{-8}
		+	1.772	0.046		35		
	PopP2	–	2.197	0.066	80	24	3.6	0.36
		+	2.117	0.058		30		
	C321A	–	2.102	0.067	229	23	10.8	1.6×10^{-2}
		+	1.873	0.063		31		
AtWRKY40-GFP	NE	–	2.222	0.034	358	30	16.0	1.8×10^{-8}
		+	1.864	0.041		43		
	PopP2	–	2.223	0.037	289	30	13.0	1.6×10^{-6}
		+	1.934	0.040		30		
	C321A	–	2.194	0.045	292	30	13.3	1.5×10^{-5}
		+	1.902	0.042		30		
RRS1-S-GFP	NE	–	2.083	0.051	297	26	14.0	1.5×10^{-4}
		+	1.786	0.050		22		
	PopP2	–	2.205	0.039	40	48	1.8	0.44
		+	2.165	0.034		50		
	C321A	–	2.190	0.030	296	41	13.5	3.5×10^{-7}
		+	1.894	0.045		36		
RRS1-S_{Cterm}-GFP	NE	–	2.162	0.032	293	30	13.5	2.9×10^{-5}
		+	1.869	0.056		30		
	PopP2	–	2.125	0.047	34	21	1.6	0.56
		+	2.091	0.037		30		
	C321A	–	2.113	0.055	316	21	14.9	1.8×10^{-4}
		+	1.797	0.053		29		
NbWRKY8-GFP	NE	–	2.095	0.029	348	30	16.6	9×10^{-12}
		+	1.746	0.028		30		
	PopP2	–	2.069	0.034	38	30	1.8	0.44
		+	2.108	0.037		30		
	C321A	–	2.089	0.024	350	30	16.7	4.6×10^{-13}
		+	1.739	0.029		30		

(legend on next page)

allowing FRET-FLIM measurements. The fluorescence lifetime of RRS1-R-GFP bound to DNA was expected to decrease significantly due to close proximity, producing transfer of energy (FRET) between the donor and acceptor molecules. No change in GFP lifetime in the presence of Sytox dye would indicate absence of close interaction with the DNA (Figure S2). Because this method relies on detection of a GFP signal with or without DNA labeling, absence of FRET cannot be due to protein instability or misexpression.

In the absence of DNA labeling, *N. benthamiana* nuclei expressing RRS1-R-GFP with GUS displayed an average GFP lifetime of 2.203 ns (Table 2). Incubation of RRS1-R-GFP with Sytox led to a significant decrease of GFP lifetime (Figure 2A; Table 2), reflecting a physical association of RRS1-R-GFP with DNA. Similar results were obtained upon co-expression of RRS1-R-GFP with C321A, which interacts physically with RRS1-R in nuclei (Tasset et al., 2010), indicating that C321A did not alter RRS1-R-GFP DNA association (Table 2). By contrast, co-expression of RRS1-R-GFP with active PopP2 produced a constant GFP lifetime before and after incubation with Sytox (Figure 2A; Table 2), indicating that PopP2 disrupts RRS1-R-GFP association with nuclear DNA. These results suggest that inhibition of RRS1-R-GFP DNA binding is a consequence of PopP2 acetyltransferase activity.

PopP2 Nε-Acetylation of Lys-1221 Disables RRS1-R DNA Binding

The WRKY DNA-binding domain recognizes a "TTGACY" DNA motif of W-box *cis*-elements in the promoters of WRKY TF target genes (Ciolkowski et al., 2008) and binds DNA in vitro (Noutoshi et al., 2005). We examined the effect of Lys-1221 acetylation on RRS1-R DNA binding to the W-box containing DNA elements in vitro using an electrophoretic mobility shift assay (EMSA). Because the GST-RRS1-R_{Cterm}-His_6 protein (Figure 1C) was difficult to elute from the GST affinity matrix, a shorter RRS1-R C-terminal portion (position 1190–1290 encompassing the WRKY domain—W^{1215}RKYGQK^{1221}), hereinafter called WRKY-R, was used to produce soluble nonacetylated or acetylated GST-tagged forms of the WRKY-R domain (GST-WRKY-R-His_6) (Figure 1D). Consistent with Noutoshi et al. (2005), purified GST-WRKY-R-His_6 bound specifically to oligomeric sequences containing W-boxes (Figure S1B). Purified nonacetylated GST-WRKY-R-His_6 co-expressed with His_6-C321A retained binding to these *cis*-elements (Figure 1D). By contrast, GST-WRKY-R-His_6 acetylated by His_6-PopP2 had impaired W-box-binding activity (Figure 1D). A mutant protein in which Lys-1221 was exchanged to nonacetylatable Arg (GST-WRKY-R-K1221R-His_6) lost W-box binding activity with PopP2 or C321A (Figure 1D). Therefore, acetylation of Lys-1221 within the RRS1-R WRKY domain (Table 1) abolishes in vitro DNA binding. Active PopP2 also disrupted RRS1-R_{Cterm}-GFP DNA association in situ (Table 2). These results show that the FRET-FLIM assay faithfully reports RRS1-R binding to DNA and that PopP2 interferes with RRS1-R WRKY DNA binding by acetylating Lys-1221 in vitro and in vivo.

PopP2 Nε-Acetylation Disrupts Electrophilic Attraction between RRS1-R and DNA

In a nuclear magnetic resonance (NMR) solution structure of a WRKY domain in complex with W-box DNA, the canonical WRKY heptad sequence contacts the DNA major groove (Yamasaki et al., 2005, 2012). The WRKY Lys residue corresponding to RRS1-R Lys-1221 contacts guanine sugar carbons by apolar interactions, hydrogen bonds, and electrostatic attraction (Yamasaki et al., 2012). To test the impact of RRS1-R WRKY domain acetylation at Lys-1221, we performed homology modeling of the RRS1-R WRKY domain (residues 1192–1273) wild-type and Lys-1221 acetylated forms bound to W-box DNA (Figure 2B). As expected, the RRS1-R WRKY domain model contacted the DNA major groove with a RKYGK^{1221} peptide within the WRKY heptad sequence. The RRS1-R Lys-1221 side chain oriented parallel to the DNA helix, forming a positively charged surface and a predicted H-bond with the DNA (Figure 2B). Substitution of Lys-1221 by acetylated Lys did not alter the RRS1-R WRKY domain carbon backbone or Lys-1221 orientation (Figure 2C). However, Lys-1221 acetylation was predicted to cause a strong decrease in electrostatic potential at the DNA interface, which would disrupt RRS1-R DNA interaction (Figure 2D).

We tested the role of electrostatic attraction in DNA binding of full-length RRS1-R protein by constructing an RRS1-R^{K1221Q} mutant in which Lys-1221 was substituted with glutamine (Q), a residue that mimics charge neutralization of the acetylated Lys (K1221Q) (Figure 2C). RRS1-R^{K1221Q} and RRS1-R^{K1221R} (Figure 1D) mutant forms fused to GFP (RRS1-R^{K1221Q}-GFP and RRS1-R^{K1221R}-GFP) were each transiently expressed in *N. benthamiana* cells without PopP2. Both fusion proteins targeted to the nucleus, allowing GFP lifetime measurements (Table 2). Incubation with Sytox did not lead to a decrease of their respective GFP lifetime, indicating that the RRS1-R^{K1221R} and RRS1-R^{K1221Q} fail to bind DNA. The K1221Q and K1221R mutations were predicted to cause a decrease in electrostatic potential at the RRS1-R WRKY domain interface with DNA (Figure 2D). These data underscore the importance of Lys-1221 for RRS1-R WRKY domain association with the chromatin. Because K1221Q and K1221R reproduced the effect of active PopP2 on RRS1-R-GFP (Figures 2C and 2D; Table 2), we concluded that PopP2 Nε-acetylation of Lys-1221 likely dislodges RRS1-R from the DNA by neutralizing the charge around Lys-1221.

NE, no effector.

[a]Mean lifetime (in nanoseconds). For each nucleus, average fluorescence decay profiles were plotted and fitted with exponential functions using a nonlinear square estimation procedure. Mean lifetime was calculated according to $\tau = \Sigma\ \alpha_i\tau_i^2/\Sigma\ \alpha_i\tau i$ with $I(t) = \Sigma\ \alpha_i\ e^{-t/\tau i}$.

[b]$\Delta t = \tau_D - \tau_{DA}$ (in nanoseconds).

[c]Total number of measured nuclei.

[d]Percentage of FRET efficiency: $E = 1 - (\tau_{DA}/\tau_D)$.

[e]The p value of the difference between the donor lifetimes in the presence and absence of acceptor (Student's t test).

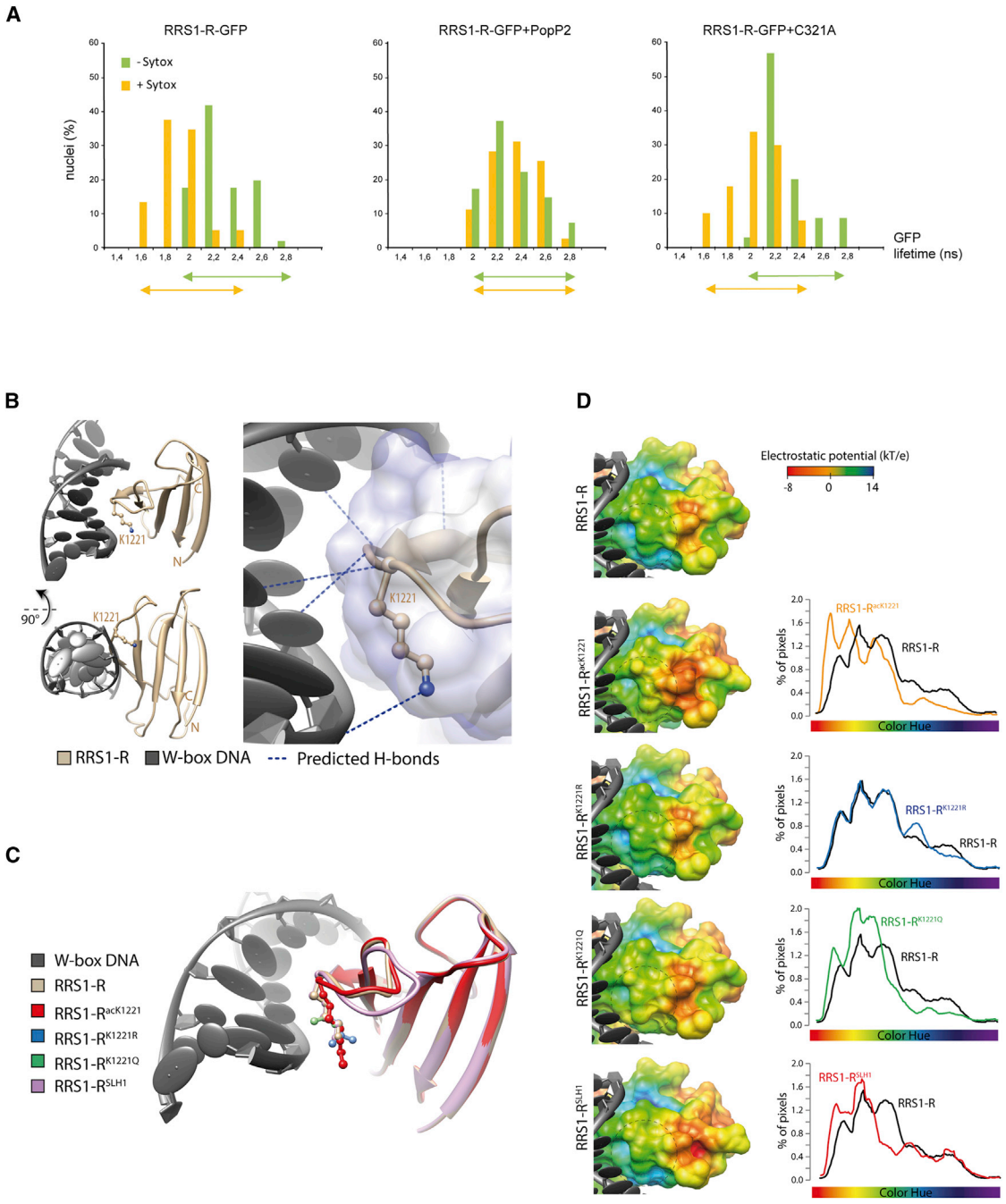

Figure 2. PopP2 Disrupts RRS1-R DNA Association In Situ

(A) GFP lifetime distribution of RRS1-R-GFP in plant nuclei expressing PopP2. Histograms show the distribution of nuclei (%) according to RRS1-R-GFP lifetime classes in the absence (green bars) or presence (orange bars) of Sytox. An overlapping GFP lifetime distribution is represented with orange (+ Sytox) and green (– Sytox) arrows.

(B) Close-up view of K1221 region showing the RRS1-R-DNA interface. Homology modeling of the RRS1-R WRKY domain (tan ribbon diagram) bound to W-box DNA (gray) highlights the central position of K1221 at the DNA. K1221 is shown as balls and sticks. Predicted H-bonds connecting the RRS1-R WRKY domain to DNA are shown as blue dotted lines.

(C) Mutations of Lys-1221 and the SLH1 insertion are predicted not to alter RRS1-R WRKY domain structure. Superimposed models of wild-type (tan), RRS1-$R^{acK1221}$ (red), RRS1-R^{K1221R} (blue), RRS1-R^{K1221Q} (green), and RRS1-R^{SLH1} (purple) WRKY domains bound to DNA are shown as ribbon diagrams, with K1221 as balls and sticks. The structure of these variants does not differ from that of the wild-type RRS1-R WRKY domain model.

(legend continued on next page)

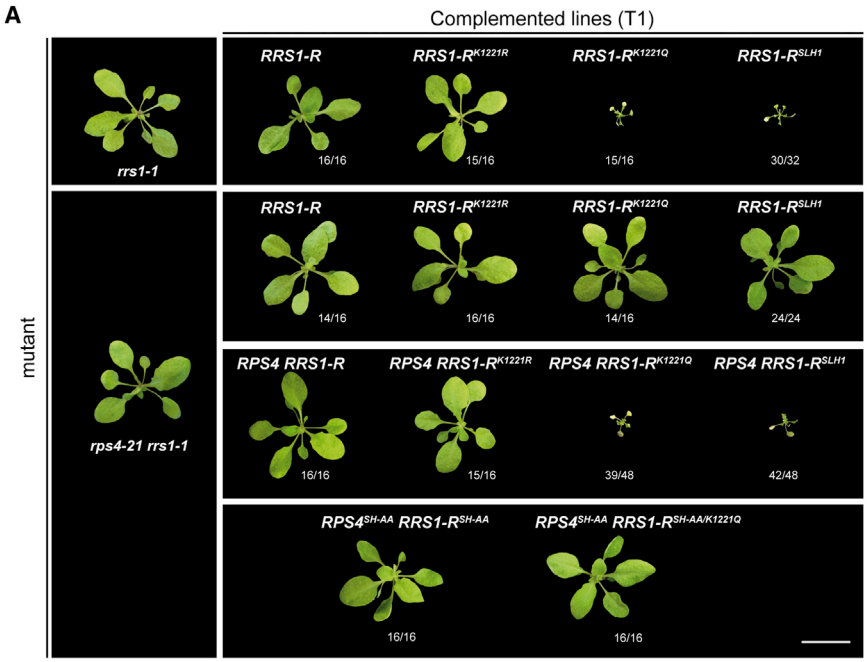

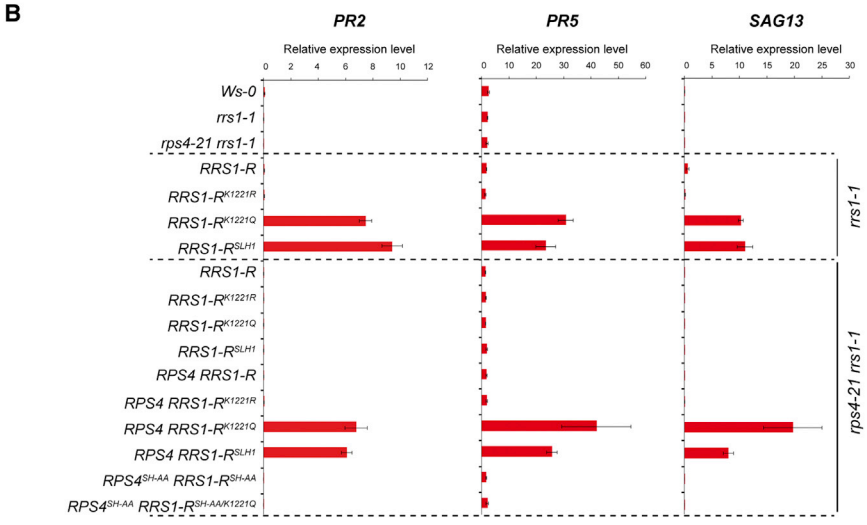

Figure 3. Mimicry of RRS1-R Acetylation by RRS1-R^{K1221Q} Activates Immunity

(A) Growth of 4-week-old *rrs1-1* and *rps4 rrs11-1* null mutants (Ws-0) untransformed or transformed with genomic clones as indicated (T1 plants). Scale bar, 2 cm. Fractions indicate the number of T1 plants displaying the shown phenotype over total number of selected plants for a given construct.

(B) Expression of *Arabidopsis* defense-related genes (*PR2*, *PR5*, and *SAG13*) monitored by qRT-PCR in the transgenic lines shown in (A). Total RNA was extracted from 4-week-old plants. Expression values are means ± SD (n = 9 from three independent transgenic lines in three independent experiments).

See also Figure S3.

RRS1-R Acetylation by PopP2 Triggers Activation of the RRS1-R/RPS4 Complex

RRS1-R behaves as a negative regulator of RPS4 activation in uninfected tissues and as the PopP2 sensor during a pathogen attack (Williams et al., 2014). Also, the *Arabidopsis rrs1 (slh1)* autoimmune mutant contains a single amino acid insertion in the RRS1-R-WRKY domain, which disrupts DNA binding in vitro (Noutoshi et al., 2005). In protein-DNA FRET-FLIM analysis, RRS1-R^{SLH1} mutant protein fused to GFP (RRS1-R^{SLH1}-GFP) failed to bind DNA, similar to RRS1-R^{K1221R} and RRS1-R^{K1221Q} mutants (Table 2). We tested whether loss of RRS1-R DNA binding, as a result of PopP2 Nε-acetylation at Lys-1221, leads to autoimmunity in *Arabidopsis*. For this, *RRS1-R* genomic clones containing the *K1221R*, *K1221Q*, or *slh1* mutations were transformed into an *rrs1-1* null mutant in *Arabidopsis* accession Ws-0 (Narusaka et al., 2009), and independent, stable T1 transgenic lines were selected. Four-week-old transgenic plants containing wild-type *RRS1-R or RRS1-R^{K1221R}* grew normally and were phenotypically similar to untransformed *rrs1-1* (Figure 3A). By contrast, transgenic lines containing either *RRS1-R^{K1221Q}* or *RRS1-R^{SLH1}* were severely stunted and developed necrotic lesions. The *Arabidopsis* defense-related genes (*PR2*, *PR5*, and *SAG13*) were strongly induced in *RRS1-R^{K1221Q}* and *RRS1-R^{SLH1}* but not in the *RRS1-R* or *RRS1-R^{K1221R}* lines, as measured by qRT-PCR (Figure 3B), and observed previously in *slh1* (Noutoshi et al., 2005). Autoimmunity of *RRS1-R^{K1221Q}* lines is, therefore, likely due to mimicry of K1221 acetylation, altering the WRKY domain electrostatic potential and DNA binding in a manner similar to that of RRS1-R^{SLH1}, rather than failure of the receptor to bind DNA, as seen for RRS1-R^{K1221R} (Figure 2D; Table 2). We concluded that PopP2 activates

(D) Lys-1221 acetylation alters predicted electrostatic potentials at the DNA interface with the RRS1-R WRKY domain. Surface electrostatic potentials (increasing from red to blue) for RRS1-R wild-type, RRS1-R^{acK1221}, RRS1-R^{K1221R}, RRS1-R^{K1221Q}, and RRS1-R^{SLH1} WRKY domains show changes in electrophily at the DNA interface. The distribution of pixels color hue is depicted in line graphs at the right of the corresponding image. Dotted circles indicate the position of K1221 in the models.

See also Figure S2.

RRS1-R immunity and defense gene expression by Nε-acetylating a critical Lys residue (Lys-1221) within the RRS1-R WRKY domain.

We tested whether *RRS1-R*^{K1221Q} autoimmunity requires *RPS4*, as shown for *Arabidopsis slh1* (Sohn et al., 2014). T1 transgenic lines containing *RRS1-R*^{K1221Q} or *RRS1*^{SLH1} in an *rps4-21 rrs1-1* null mutant (Narusaka et al., 2009) were phenotypically similar to untransformed *rps4-21 rrs1-1* plants and did not display constitutive defense gene expression (Figures 3A and 3B). By contrast, *rps4 rrs1-1* transformed with *RPS4 RRS1-R*^{K1221Q} or *RPS4 RRS1-R*^{SLH1} genomic clones exhibited autoimmunity (Figures 3A and 3B). Expression of the *RRS1-R* and/or *RPS4* transgenes was verified in independent transgenics by qRT-PCR (Figure S3A). Transgenically expressed *RPS4*$^{SH-AA}$ *RRS1-R*$^{SH-AA/K1221Q}$ carrying K1221Q, as well as SH-AA mutations in the RPS4 and RRS1-R TIR domains that disrupt TIR domain heterodimerization and receptor signaling (Williams et al., 2014), also failed to activate immunity (Figures 3A and 3B). Therefore, RRS1-R^{K1221Q} autoimmunity involves interaction between RRS1-R and RPS4 TIR domains.

PopP2 Acetylates Multiple Host WRKY TFs

Because the RRS1-R WRKY domain is a PopP2 acetyltransferase substrate (Figure 1; Table 1) we explored whether WRKY TFs are acetylated by PopP2 to aid bacterial infection, since many of the 74 WRKY TFs in *Arabidopsis* have stress-related functions (Rushton et al., 2010). Plant WRKY TFs fall into three main groups (I, II, and III) and several subgroups, based on their number of WRKY DNA-binding domains and type of zinc finger motif (Rushton et al., 2010). We selected WRKY-coding DNA sequences from the different groups: AtWRKY25 (group I); AtWRKY18, -40, and -60 (group IIa); AtWRKY28 and -71 (group IIc); AtWRKY22, -27, and -29 (group IIe); and AtWRKY38, -41, and -53 (group III, to which RRS1-R belongs). Corresponding C-terminal GFP fusions (AtWRKY-GFP) were each co-expressed with GUS, PopP2, or C321A tagged with 3HA in *N. benthamiana* transient assays. Accumulation of the WRKY-GFP proteins, as well as co-expressed GUS-HA, PopP2-HA, or C321A-HA, was monitored on immunoblots probed with anti-GFP and anti-HA antibodies, respectively (Figure 4). Both PopP2 and C321A promote RRS1-R accumulation, presumably by modulating proteasome degradation (Tasset et al., 2010). Similarly, 9 of the 12 WRKYs tested showed a tendency toward higher accumulation in the presence of PopP2 and/or C321A (Figure 4). Lys acetylation of the immuno-purified WRKY-GFP proteins was monitored on immunoblots with anti-Ac-K antibodies. Ten of the 12 WRKY TFs tested were acetylated in a PopP2-dependent manner (Figure 4). Using the bacterial in vitro acetylation assay, acetylation of selected WRKY proteins (AtWRKY14, -22, -26, and -30) was also detected upon co-expression with active PopP2 but not C321A (Figure S4A).

Lys Acetylation by PopP2 Inhibits WRKY TF-DNA Binding

We examined whether PopP2-triggered acetylation of WKRY TFs affects their binding to DNA. From the ten WRKY proteins identified as acetylated by PopP2 in *N. benthamiana* (Figure 4), we selected AtWRKY22 (group IIe), which is a component of *Arabidopsis* immunity (Asai et al., 2002), and performed FRET-FLIM measurements of AtWRKY22 fused to GFP (AtWRKY22-GFP) and transiently expressed in *N. benthamiana*. The AtWRKY22-GFP FRET lifetime indicated AtWRKY22-GFP physical association with the nuclear DNA, and this interaction was inhibited by PopP2 (Table 2). A mass spectrometric analysis of immuno-purified AtWRKY22 co-expressed with PopP2 or C321A in *N. benthamiana* (AtWRKY22-GFP) or in *E. coli* (GST-AtWRKY22-His$_6$) revealed that the last Lys of its WRKY heptad motif (Lys-139) was acetylated by PopP2 (WRKYGQ-acK^{139}; see Tables 1 and S1). Substituting AtWRKY22 Lys-139 with Arg (AtWRKY22^{K139R}) impaired AtWRKY22 acetylation by PopP2 in the bacterial acetylation assay (Figure S4B), indicating that Lys-139 is the principal AtWRKY22 residue targeted for PopP2 acetylation in *E. coli*. Similar results were obtained using recombinant AtWRKY53 (group III) and AtWRKY53^{K169R} with the last Lys of its WRKY heptad exchanged to Arg (Figure S4B). Microsequencing of immuno-purified GST-tagged AtWRKY30 (group III), which was acetylated by PopP2 in bacterial cells (Figure S4A), also revealed acetylation of the last WRKY heptad Lys residue (WRKYGQ-acK^{124}; Tables 1 and S1). Collectively, the data show that the final Lys of the WRKY heptad motif in different WRKY TFs is acetylated by PopP2.

Notably, two WRKY TFs (AtWRKY40 and AtWRKY60) were not acetylated upon co-expression with active PopP2 in the *N. benthamiana* transient assay (Figure 4). Similarly, co-expression of GST-AtWRKY40 recombinant protein with PopP2 in *E. coli* did not result in AtWRKY40 acetylation (Figure S4A). A mass spectrometric analysis performed on AtWRKY40 immuno-purified from plant or *E. coli* extracts confirmed the absence of an acetylated residue in the AtWRKY40 WRKY heptad (Tables 1 and S1). Failure of PopP2 to acetylate AtWRKY40 (Figures 4 and S4A) correlated with its inability to disrupt AtWRKY40 DNA binding in plant nuclei, as indicated by FRET-FLIM measurements (Table 2). These observations suggest that the presence of a WRKY domain does not automatically lead to its modification by PopP2 and, hence, a degree of PopP2 substrate specificity. Protein folding and/or the nature of sequences flanking the WRKY domain might alter binding of acetyl-coenzyme A (CoA) to the last Lys of the WRKY heptad. Using the bacterial in vitro acetylation assay, acetylation of AtWRKY40 (position 112–161)-, AtWRKY60 (position 112–161)-, or RRS1-R (position 1225–1178)-truncated domains, all containing the WRKY heptad, was detected upon co-expression with active PopP2 (Figure S4C). Therefore, sequences outside the WRKY domains likely affect accessibility to PopP2 transacetylation.

PopP2 Contributes to *Ralstonia solanacearum* Virulence

In the absence of PopP2 recognition, we postulated that PopP2 acetylation of host WRKY TFs contributes to *R. solanacearum* pathogenicity. To test this, *R. solanacearum* strains delivering PopP2-3HA (*Rs*PopP2) or C321A-HA (*Rs*C321A) variants that are discriminated by RRS1-R in resistance (Tasset et al., 2010) were inoculated onto the roots of *Arabidopsis* Col-0 plants containing the *RRS1-S* allelic form that does not trigger immunity to PopP2 (Deslandes et al., 2002, 2003). In the root infection assays, *Rs*PopP2 provoked faster and stronger bacterial wilt symptoms than *Rs*C321A or a *R. solanacearum* PopP2 deletant

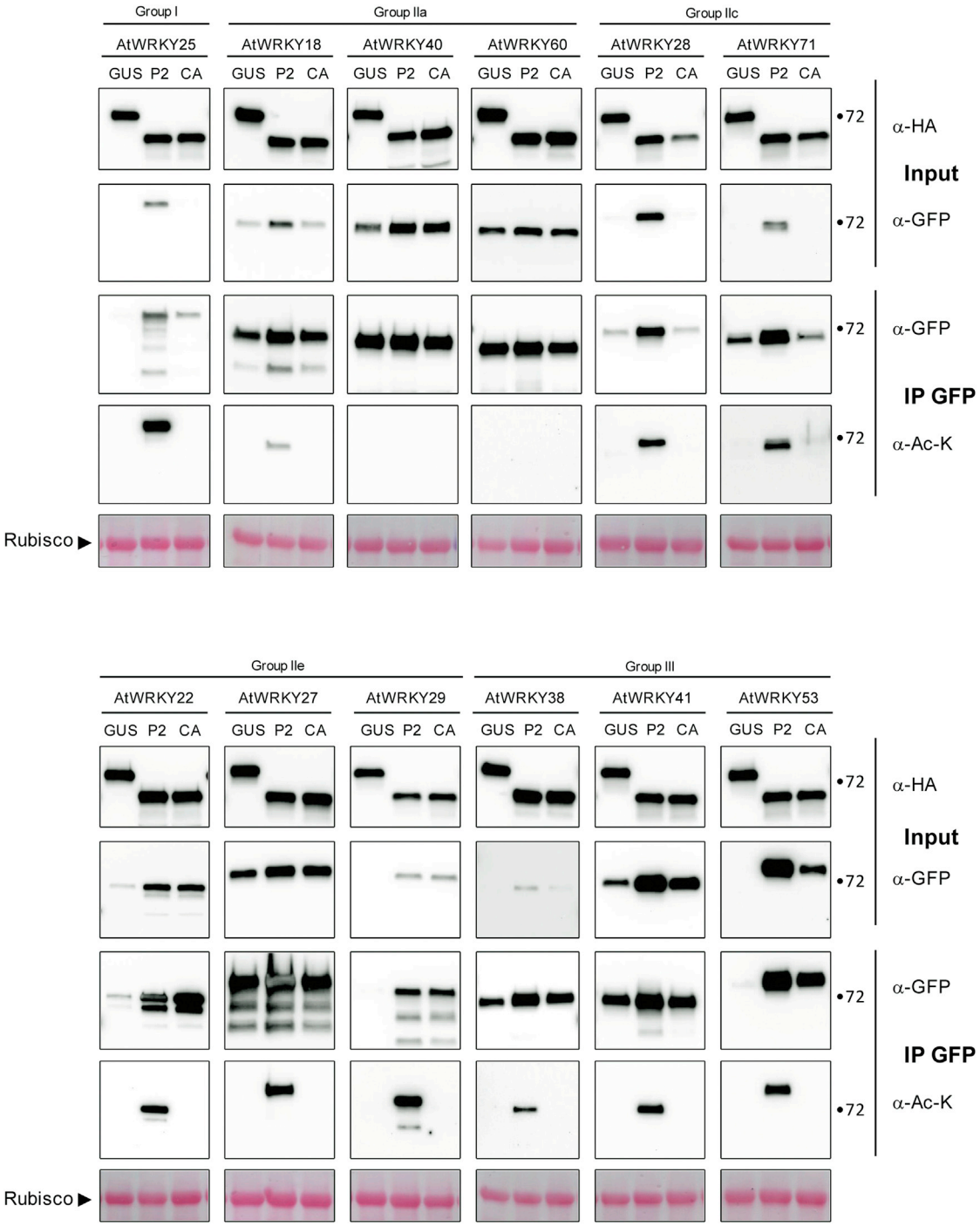

Figure 4. PopP2 Directly Acetylates Multiple *Arabidopsis* WRKY TFs

AtWRKY25 (group I); -18, -40, and -60 (group IIa); -28 and -71 (group IIc); -22, -27, and -29 (group IIe); and -38, -41, and -53 (group III) fused to GFP (AtWRKY-GFP) were transiently co-expressed with 3HA-tagged GUS, PopP2, or C321A in *N. benthamiana* leaves. Acetylated WRKY proteins were detected as described in Figure 1A. Rubisco is shown as a loading control (bottom). Results were consistent in three independent experiments.
See also Figure S4.

strain (Δ*PopP2*) (Figure S3B). Therefore, PopP2 acetyltransferase activity contributes to *R. solanacearum* disease in *Arabidopsis*.

Strikingly, we found that active PopP2, but not C321A, acetylates RRS1-S at the same Lys residue identified in the RRS1-R WRKY domain (Figures S1C and S1D; Tables 1 and S1). Also,

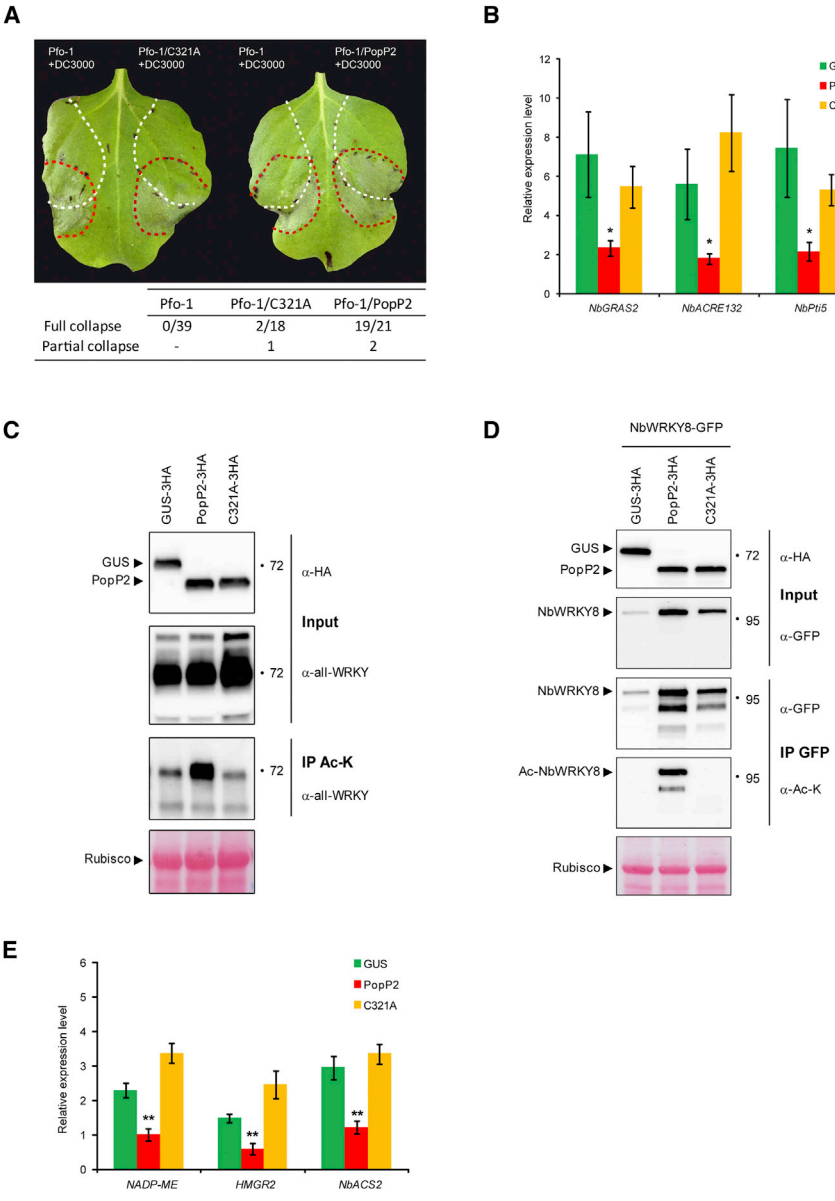

Figure 5. PopP2 Activity Disables WRKY Transactivating Functions Needed for Defense Gene Expression and Disease Resistance

(A and B) PopP2 inhibits PTI in *N. benthamiana*. Suspensions of Pfo-1 wild-type strain or Pfo-1-expressing PopP2-3HA or C321A-3HA were infiltrated into *N. benthamiana* leaves (white dotted line). After 7 hr, a suspension of *P. syringae* DC3000 was infiltrated in an overlapping area (red dotted line). Values indicate the frequency of tissue collapse at 48 hr post-inoculation in overlapping areas of leaves from four independent experiments. (B) shows that Flg22-induced expression of *NbGRAS2*, *NbACRE132*, and *NbPti5* PTI marker genes is reduced in *N. benthamiana* cells transiently expressing PopP2. Expression values are means ± SD (n = 4 for each condition from at least two independent experiments; *p < 0.05; Student's t test).

(C) Acetylation of native NbWRKY TFs by PopP2. 3HA-tagged GUS, PopP2, and C321A were transiently expressed in *N. benthamiana* leaves. Protein extracts were analyzed by immunoblotting with α-HA and α-all-WRKY antibodies. IP was performed with α-acetyl-lysine antibodies (IP Ac-K), and proteins were analyzed by immunoblotting with α-all-WRKY antibodies. Rubisco is shown as loading control (bottom). Results were consistent in three independent experiments.

(D) PopP2 acetylates NbWRKY8. NbWRKY8-GFP was transiently co-expressed with 3HA-tagged GUS, PopP2, or C321A in *N. benthamiana* leaves. Acetylated NbWRKY8 protein (Ac-NbWRKY8) was detected as described in Figure 1A. Rubisco is shown as a loading control (bottom). Results were consistent in three independent experiments.

(E) PopP2 interferes with NbWRKY8 transactivating activity. Flg22-induced upregulation of NbWRKY8 target genes *NADP-ME*, *HMGR2*, and *NbACS2* decreases in the presence of active PopP2. Expression values are means ± SD (n = 4 for each condition from at least two independent experiments; **p < 0.01; Student's t test).

See also Figure S5.

active PopP2 disrupts RRS1-S DNA association in plant nuclei (Table 2). These data suggest that the lack of RRS1-S resistance to PopP2 is not because PopP2 fails to disrupt RRS1-S DNA binding.

PopP2 Acetylation of WRKY TFs Dampens PTI

We considered whether PopP2-triggered acetylation of multiple plant host WRKY TFs might be a broadly effective bacterial virulence strategy to dampen defense reprogramming in favor of infection. Because WRKY TFs positively regulate basal disease resistance in *N. benthamiana* (Ishihama et al., 2011; Zhang et al., 2012), we tested whether catalytically active PopP2 interferes with PTI using an *N. benthamiana* cell-death assay (Oh and Collmer, 2005). Briefly, PTI induction by an infiltrated non-pathogenic bacterial strain can suppress a localized ETI necrotic response elicited by subsequent infiltration of a pathogenic bacterial strain. If the non-pathogenic bacterium delivers a PTI-suppressing effector, cell death occurs in the area infiltrated with the pathogenic strain (Badel et al., 2013). PopP2 or C321A were delivered as 3HA-tagged proteins via the type III secretion system (TTSS) of a *Pseudomonas fluorescens* (Pfo-1) non-pathogenic strain (Figure S5A). Infiltration of *N. benthamiana* leaves with wild-type Pfo-1 or Pfo-1-delivering C321A-3HA (Pfo-1/C321A) did not inhibit PTI, as indicated by an absence of tissue collapse in the leaf area subsequently infiltrated with the recognized *P. syringae* pv. *tomato* strain DC3000 (DC3000) (Figure 5A). In areas pre-infiltrated with Pfo-1-delivering active PopP2-3HA (Pfo-1/PopP2), we observed a cell-death ETI response to DC3000 (Figure 5A), suggesting that PopP2 acetyltransferase activity dampens host PTI. We tested whether PopP2 affects the

expression of PTI marker genes by treating *N. benthamiana* cells expressing GUS, PopP2, or C321A (Figure S5B) with the bacterial PAMP, flg22. Three tested PTI marker genes (*NbGRAS2*, *NbACRE132*, and *NbPti5*) were upregulated after flg22 treatment in plant cells expressing GUS or C321A (Figure 5B). By contrast, flg22-induced upregulation of the marker genes was reduced in leaf tissues expressing active PopP2 (Figure 5B). Together, the data show that PopP2 acetylation activity contributes to PTI suppression.

Immunoprecipitation (IP) of acetylated endogenous *N. benthamiana* WRKY TFs using anti-acetyl Lys antibodies and immunoblotting with anti-all-WRKY antibodies suggest that PopP2 dampening of PTI involves acetylation of multiple NbWRKYs, since a much stronger WRKY protein signal was observed upon expression of PopP2 compared to GUS or C321A (Figure 5C). Our data suggest a direct link between the disabling of PTI and WRKY TF acetylation by active PopP2.

PopP2-Acetylated NbWRKY8 Has Impaired Defense Gene Transactivation Activity

To test whether PopP2 inhibition of WRKY TF DNA binding directly affects host defense gene expression, we examined the transactivation activity of NbWRKY8, a previously characterized group I WRKY TF from *N. benthamiana*, which promotes defense gene induction (Ishihama et al., 2011) and is acetylated by PopP2 (Figure 5D). Using flg22-treated leaf material described earlier for the PTI inhibition assay (Figure 5B), we found that *NbWRKY8* was upregulated to similar levels in the presence of GUS, PopP2, or C321A (Figure S5C). In this material, we measured Flg22-induced expression of two known NbWRKY8-transactivated target genes: *NADP-ME* (*NADP-malic enzyme*) and *HMGR2* (*3-hydroxy-3-methylglutaryl CoA reductase 2*) (Ishihama et al., 2011). We also tested the effect of PopP2 on flg22-induced expression of *ACS2* (*1-amino-cyclopropane-1-carboxylic acid synthase 2*) in *N. benthamiana*. AtWRKY33, an ortholog of NbWRKY8, was shown to directly bind to W-boxes in the promoter region of *AtACS2* and to positively regulate its expression (Li et al., 2012), suggesting that NbWRKY8 also upregulates *NbACS2*. Whereas samples expressing GUS or C321A exhibited upregulation of *NADP-ME*, *HMGR2*, and *NbACS2* (Figure 5E), samples with active PopP2 had strongly diminished flg22-induced expression of these genes (Figure 5E). These data suggest that PopP2 acetylation of endogenous NbWRKY8 impairs its transactivating activity (Figure 5D). In the *N. benthamiana* FRET-FLIM assay, NbWRKY8-GFP association with DNA was inhibited by co-expressed PopP2 but not C321A (Table 2). Collectively, our data suggest that PopP2 acetylation of multiple defense-acting WRKY TFs dislodges them from the DNA, thereby reducing defense gene activation.

DISCUSSION

Here, we describe a broad-ranging bacterial virulence activity targeting multiple plant host WRKY TFs to dampen immunity (Figures 4 and 5). This pathogen-interference mechanism is sensed at the chromatin by a WRKY-domain-containing NLR receptor, turning defense suppression into immunity (Figure 3).

PopP2 Uses Nε-Acetylation to Alter Eukaryotic TF-DNA Binding

Reprogramming of gene transcription is necessary for mobilizing host defenses, and many bacterial effectors modulate transcription (Rivas and Deslandes, 2013). Bacterial strategies include the inhibition of RNA-binding proteins that enhance expression of immunity-related RNAs (Nicaise et al., 2013) and direct transcriptional activation of host genes benefiting pathogen growth and dissemination (Boch et al., 2009). Effectors also target host TFs, although the underlying defense-manipulation mechanisms remain obscure. *R. solanacearum* PopP2 uses acetylation to inhibit DNA-binding activities of plant-defensive WRKY TFs (Table 2), thereby disabling their transcriptional functions (Figure 5). Across prokaryotes and eukaryotes, Nε-Lys acetylation alters TF sequence-specific DNA binding (Matsuzaki et al., 2005; Thao et al., 2010). Therefore, PopP2 has subverted an evolutionary conserved mechanism to manipulate host defenses and promote pathogen infection. This molecular strategy is different from known modes of action of YopJ-like family effectors, which, in mammalian cells and *Drosophila*, acetylate critical serine and threonine residues of immune signaling kinases to inhibit activities and/or disturb associations with immune receptors (Jones et al., 2008; Meinzer et al., 2012).

PopP2 Targets Host WRKY TFs to Disable Defense

Multiple lines of evidence place WRKY TFs at the heart of the plant innate immune system, mediating PTI, ETI, and systemic acquired resistance (SAR) responses (Eulgem and Somssich, 2007; Rushton et al., 2010). Identification of AtWRKY22 and AtWRKY29 as PopP2 substrates (Figure 4) strengthens the idea that their manipulation contributes to pathogen infection because these WRKYs promote PAMP-induced MAPK (mitogen-activated protein kinase) signaling in *Arabidopsis* resistance to bacterial and fungal pathogens (Asai et al., 2002). Two additional PopP2 substrates, AtWRKY27 and AtWRKY53 (Figure 4), contribute to *R. solanacearum* disease progression in the absence of NLR recognition (Hu et al., 2008; Mukhtar et al., 2008). Therefore, AtWRKY27 and AtWRKY53 behave as PopP2 virulence targets whose manipulation by PopP2 likely facilitates bacterial infection.

Selective Acetylation of WRKY TFs by PopP2

PopP2 targeted the conserved WRKYGQK heptad element of WRKY proteins but did not acetylate or dislodge from the DNA all tested members of the WRKY superfamily, since full-length AtWRKY40 and AtWRKY60 were refractory to PopP2 activity (Figures 4 and S4A; Tables 1 and 2). AtWRKY40 and AtWRKY60, together with AtWRKY18, negatively regulate *Arabidopsis* resistance to virulent *P. syringae* bacteria (Xu et al., 2006). AtWRKY18 was acetylated by PopP2 (Figure 4) and alone appears to have a positive regulatory role in SAR (Wang et al., 2006). Selective targeting of WRKYs by PopP2 suggests that the effector has evolved a degree of substrate discrimination, potentially to avoid negative defense components whose inactivation would be disadvantageous for bacterial infection.

RRS1-R Integrates an Effector Decoy with an NLR Receptor/Signaling Pair

The *Arabidopsis* RRS1-R RPS4 NLR pair forms a functional receptor recognition/signaling complex through homo- and hetero-dimerization involving their respective TIR domains (Griebel et al., 2014; Williams et al., 2014). PopP2 associates with RRS1-R in the RRS1-R RPS4 complex (Tasset et al., 2010; Williams et al., 2014). Here, we show that PopP2 acetylates a Lys residue in the RRS1-R WRKY domain that disrupts RRS1-R DNA association and activates RPS4-dependent immunity (Figures 1 and 3; Tables 1 and 2). An insertion within the WRKY domain of RRS1-R that abolishes DNA binding in vitro constitutively activates immunity (Noutoshi et al., 2005), consistent with RRS1-R acting as a negative regulator of RPS4 in an auto-inhibited hetero-complex at the chromatin. We infer from our data that PopP2 direct acetylation disengages RRS1-R from its position on the DNA by altering WRKY domain electrostatic potential, thereby reorienting RRS1-R RPS4 to release a signaling active NLR receptor complex (Figure 3). Because WRKY TFs serve as PopP2 substrates, we propose that RRS1-R has integrated a decoy—namely, the WRKY domain—with an NLR molecular switch to directly capture effector virulence activity at the chromatin. This sensor system thus betrays a fundamental effector enzymatic activity that cannot easily be dispensed with by the pathogen unless it evolves a different host interference mechanism. The RRS1-R RPS4 NLR pair also confers recognition of *P. syringae* AvrRps4, which is unrelated to PopP2 (Sohn et al., 2012) but associates with the RRS1 WRKY domain and with several WRKY TFs (Sarris et al., 2015). Therefore, bacterial pathogens likely use different effector molecules to interfere with WRKY TF-controlled defenses, and these are intercepted by the RRS1-R RPS4 receptor complex.

Unexpectedly, the RRS1-S receptor natural variant that does not trigger resistance to PopP2 (Deslandes et al., 2002) is acetylated by active PopP2 at the same critical Lys within the RRS1-S WRKY domain (Figures S1C and S1D; Table 1), causing a loss of RRS1-S DNA binding (Table 2). Therefore, as measured by these assays, absence of RRS1-S resistance to PopP2 (Deslandes et al., 2002) is not due to a failure of PopP2 modification or perturbation of RRS1-S DNA binding. The most obvious difference between RRS1-R and RRS1-S is the presence of 90 additional residues at the RRS1-R C terminus (Deslandes et al., 2002), which might confer binding to a particular set of target defense genes or interactors required for resistance signaling.

Some nuclear NLRs cooperate with TFs in ETI (Chang et al., 2013; Inoue et al., 2013). Barley MLA10 interferes directly with interactions between two antagonistically acting TFs, WRKY1 and MYB6, to stimulate defense gene expression in resistance to *Blumeria graminis* f. sp. *hordei* (Chang et al., 2013). In rice, resistance to *Magnaporthe oryzae* involves physical association between the NLR Pb1 (Panicle blast1) and WRKY45, a transcriptional activator of defense responses (Inoue et al., 2013). By incorporating an effector target and molecular switch in one molecule, RRS1-R physically connects effector recognition with NLR activation, leading to transcriptional reprogramming.

In rice, recognition of the AVR1-CO39 effector from *Magnaporthe oryzae* requires molecular cooperation between NLRs RGA4 and RGA5, which form a cytoplasmic receptor complex (Césari et al., 2014). Notably, RGA5 possesses an atypical C-terminal effector-targeted domain with structural similarity to a *Saccharomyces cerevisiae* copper-binding protein, ATX1 (RATX1 domain) (Cesari et al., 2013). The RATX1 domain in RGA5 likely serves as another integrated decoy for effectors targeting RATX1-containing proteins to promote pathogenicity.

EXPERIMENTAL PROCEDURES

Additional information regarding bacterial strains, plant materials, molecular constructs, *N. benthamiana* transient assays, IPs, mass spectrometry analyses, WRKY domain modeling, qRT-PCR, and PTI inhibition assays is provided in the Supplemental Experimental Procedures.

Bacterial Acetylation Assays

Production of recombinant acetylated proteins was performed as previously described (Tasset et al., 2010), with some modifications (see Supplemental Experimental Procedures).

Electromobility Shift Assays

A Pierce LightShift Chemiluminescent EMSA kit was used, with minor modifications (see Supplemental Experimental Procedures).

N. benthamiana Transient Expression Assays

For *N. benthamiana* transient expression, *A. tumefaciens* strains grown in YEB medium were centrifuged and incubated for 1 hr in 10 mM MES (pH 5.6), 10 mM $MgCl_2$, 150 μM acetosyringone (optical density 600 [OD_{600}] = 0.25). Leaf disc samples were harvested after 48 hr.

Preparation of Leaf Samples for FRET-FLIM Analysis

A. tumefaciens-infiltrated *N. benthamiana* leaf disc samples (8-mm diameter, harvested 48 hr post-infiltration) were vacuum infiltrated in fixation solution (4% w/v) paraformaldehyde and 0.05 M $(CH_3)_2AsO_2Na$ and incubated for 20 min at 4°C. Samples were rinsed in TBS buffer (25 mM Tris-HCl (pH 7.5), 140 mM NaCl, 3 mM KCl) for 5 min. Permeabilization of fixed samples was performed by incubation in proteinase K buffer (50 mM Tris-HCl (pH 7.5), 100 mM NaCl, 1 mM EDTA, 0.5% SDS, 200 μg/ml of proteinase K, Invitrogen) for 10 min at 37°C. Samples were rinsed in TBS buffer for 5 min. Nucleic acid staining was performed by vacuum infiltrating a 5-μM Sytox Orange (Invitrogen) solution (TBS buffer) and incubating samples for 30 min at room temperature in the dark. Fixed leaf discs were washed with and mounted on TBS buffer before observations on an inverted microscope (Eclipse TE2000E, Nikon). FRET-FLIM measurements were performed as previously described (Tasset et al., 2010) with some modifications (see Supplemental Experimental Procedures).

SUPPLEMENTAL INFORMATION

Supplemental Information includes Supplemental Experimental Procedures, five figures, and two tables and can be found with this article online at http://dx.doi.org/10.1016/j.cell.2015.04.025.

AUTHOR CONTRIBUTIONS

L.D. designed the project; C.L.R., G.H., A.J., D.T., L.C., B.Z., M.L., H.A., R.B., A.K., Y.C., and L.D. performed experiments; S.R. did the protein modeling; C.L.R., G.H., H.Y., R.B., D.T., J.E.P., and L.D. analyzed data; L.D. and J.E.P. wrote the manuscript with comments from all authors.

ACKNOWLEDGMENTS

We thank I. Somssich and B. Ülker for providing anti-all-WRKY antibodies and AtWRKY clones. We also thank D. Rengel for help with statistical tests and Y. Marco for insightful comments on the manuscript. L.D. and G.H. were supported by a research grant from the Agence Nationale pour la Recherche

(ANR; ANR-10-JCJC-1706). C.L.R. was funded by fellowships from INRA Contrat Jeune Scientifique and the Max Planck Society. This work was supported by the French Laboratory of Excellence project "TULIP" (ANR-10-LABX-41; ANR-11-IDEX-0002-02). A.K. and Y.C. were supported by the CNRS, INSERM, CEA, and ANR (Investissement d'Avenir Infrastructures, ProFi project ANR-10-INBS-08-01). H.Y. is supported by Grant-in-Aid from Japan Society of the Promotion of Science (26292023). S.R. is supported by a Starting Grant of the European Research Council (ERC-StG 336808 project VariWhim). J.E.P. is supported by the Max-Planck Society, DFG SFB grant 670, and the Cluster of Excellence on Plant Sciences (CEPLAS).

Received: October 17, 2014
Revised: February 4, 2015
Accepted: April 3, 2015
Published: May 21, 2015

REFERENCES

Asai, T., Tena, G., Plotnikova, J., Willmann, M.R., Chiu, W.L., Gomez-Gomez, L., Boller, T., Ausubel, F.M., and Sheen, J. (2002). MAP kinase signalling cascade in *Arabidopsis* innate immunity. Nature *415*, 977–983.

Badel, J.L., Piquerez, S.J., Greenshields, D., Rallapalli, G., Fabro, G., Ishaque, N., and Jones, J.D. (2013). In planta effector competition assays detect Hyaloperonospora arabidopsidis effectors that contribute to virulence and localize to different plant subcellular compartments. Mol. Plant Microbe Interact. *26*, 745–757.

Boch, J., Scholze, H., Schornack, S., Landgraf, A., Hahn, S., Kay, S., Lahaye, T., Nickstadt, A., and Bonas, U. (2009). Breaking the code of DNA binding specificity of TAL-type III effectors. Science *326*, 1509–1512.

Cesari, S., Thilliez, G., Ribot, C., Chalvon, V., Michel, C., Jauneau, A., Rivas, S., Alaux, L., Kanzaki, H., Okuyama, Y., et al. (2013). The rice resistance protein pair RGA4/RGA5 recognizes the Magnaporthe oryzae effectors AVR-Pia and AVR1-CO39 by direct binding. Plant Cell *25*, 1463–1481.

Césari, S., Kanzaki, H., Fujiwara, T., Bernoux, M., Chalvon, V., Kawano, Y., Shimamoto, K., Dodds, P., Terauchi, R., and Kroj, T. (2014). The NB-LRR proteins RGA4 and RGA5 interact functionally and physically to confer disease resistance. EMBO J. *33*, 1941–1959.

Chang, C., Yu, D., Jiao, J., Jing, S., Schulze-Lefert, P., and Shen, Q.H. (2013). Barley MLA immune receptors directly interfere with antagonistically acting transcription factors to initiate disease resistance signaling. Plant Cell *25*, 1158–1173.

Ciolkowski, I., Wanke, D., Birkenbihl, R.P., and Somssich, I.E. (2008). Studies on DNA-binding selectivity of WRKY transcription factors lend structural clues into WRKY-domain function. Plant Mol. Biol. *68*, 81–92.

Cremazy, F.G., Manders, E.M., Bastiaens, P.I., Kramer, G., Hager, G.L., van Munster, E.B., Verschure, P.J., Gadella, T.J., Jr., and van Driel, R. (2005). Imaging in situ protein-DNA interactions in the cell nucleus using FRET-FLIM. Exp. Cell Res. *309*, 390–396.

Deslandes, L., Olivier, J., Theulieres, F., Hirsch, J., Feng, D.X., Bittner-Eddy, P., Beynon, J., and Marco, Y. (2002). Resistance to Ralstonia solanacearum in Arabidopsis thaliana is conferred by the recessive RRS1-R gene, a member of a novel family of resistance genes. Proc. Natl. Acad. Sci. USA *99*, 2404–2409.

Deslandes, L., Olivier, J., Peeters, N., Feng, D.X., Khounlotham, M., Boucher, C., Somssich, I., Genin, S., and Marco, Y. (2003). Physical interaction between RRS1-R, a protein conferring resistance to bacterial wilt, and PopP2, a type III effector targeted to the plant nucleus. Proc. Natl. Acad. Sci. USA *100*, 8024–8029.

Dodds, P.N., and Rathjen, J.P. (2010). Plant immunity: towards an integrated view of plant-pathogen interactions. Nat. Rev. Genet. *11*, 539–548.

Eulgem, T., and Somssich, I.E. (2007). Networks of WRKY transcription factors in defense signaling. Curr. Opin. Plant Biol. *10*, 366–371.

Griebel, T., Maekawa, T., and Parker, J. (2014). Nucleotide-binding oligomerization domain-like receptor cooperativity in effector-triggered immunity. Trends Immunol. *35*, 562–570.

Hinsch, M., and Staskawicz, B. (1996). Identification of a new Arabidopsis disease resistance locus, RPs4, and cloning of the corresponding avirulence gene, avrRps4, from Pseudomonas syringae pv. pisi. Mol. Plant Microbe Interact. *9*, 55–61.

Hu, J., Barlet, X., Deslandes, L., Hirsch, J., Feng, D.X., Somssich, I., and Marco, Y. (2008). Transcriptional responses of Arabidopsis thaliana during wilt disease caused by the soil-borne phytopathogenic bacterium, Ralstonia solanacearum. PLoS ONE *3*, e2589.

Inoue, H., Hayashi, N., Matsushita, A., Xinqiong, L., Nakayama, A., Sugano, S., Jiang, C.J., and Takatsuji, H. (2013). Blast resistance of CC-NB-LRR protein Pb1 is mediated by WRKY45 through protein-protein interaction. Proc. Natl. Acad. Sci. USA *110*, 9577–9582.

Ishihama, N., Yamada, R., Yoshioka, M., Katou, S., and Yoshioka, H. (2011). Phosphorylation of the Nicotiana benthamiana WRKY8 transcription factor by MAPK functions in the defense response. Plant Cell *23*, 1153–1170.

Jiang, S., Yao, J., Ma, K.W., Zhou, H., Song, J., He, S.Y., and Ma, W. (2013). Bacterial effector activates jasmonate signaling by directly targeting JAZ transcriptional repressors. PLoS Pathog. *9*, e1003715.

Jones, J.D., and Dangl, J.L. (2006). The plant immune system. Nature *444*, 323–329.

Jones, R.M., Wu, H., Wentworth, C., Luo, L., Collier-Hyams, L., and Neish, A.S. (2008). Salmonella AvrA coordinates suppression of host immune and apoptotic defenses via JNK pathway blockade. Cell Host Microbe *3*, 233–244.

Kanzaki, H., Yoshida, K., Saitoh, H., Fujisaki, K., Hirabuchi, A., Alaux, L., Fournier, E., Tharreau, D., and Terauchi, R. (2012). Arms race co-evolution of Magnaporthe oryzae AVR-Pik and rice Pik genes driven by their physical interactions. Plant J. *72*, 894–907.

Lewis, J.D., Lee, A.H., Hassan, J.A., Wan, J., Hurley, B., Jhingree, J.R., Wang, P.W., Lo, T., Youn, J.Y., Guttman, D.S., and Desveaux, D. (2013). The Arabidopsis ZED1 pseudokinase is required for ZAR1-mediated immunity induced by the Pseudomonas syringae type III effector HopZ1a. Proc. Natl. Acad. Sci. USA *110*, 18722–18727.

Li, G., Meng, X., Wang, R., Mao, G., Han, L., Liu, Y., and Zhang, S. (2012). Dual-level regulation of ACC synthase activity by MPK3/MPK6 cascade and its downstream WRKY transcription factor during ethylene induction in Arabidopsis. PLoS Genet. *8*, e1002767.

Maekawa, T., Kufer, T.A., and Schulze-Lefert, P. (2011). NLR functions in plant and animal immune systems: so far and yet so close. Nat. Immunol. *12*, 817–826.

Matsuzaki, H., Daitoku, H., Hatta, M., Aoyama, H., Yoshimochi, K., and Fukamizu, A. (2005). Acetylation of Foxo1 alters its DNA-binding ability and sensitivity to phosphorylation. Proc. Natl. Acad. Sci. USA *102*, 11278–11283.

Meinzer, U., Barreau, F., Esmiol-Welterlin, S., Jung, C., Villard, C., Léger, T., Ben-Mkaddem, S., Berrebi, D., Dussaillant, M., Alnabhani, Z., et al. (2012). Yersinia pseudotuberculosis effector YopJ subverts the Nod2/RICK/TAK1 pathway and activates caspase-1 to induce intestinal barrier dysfunction. Cell Host Microbe *11*, 337–351.

Mittal, R., Peak-Chew, S.Y., and McMahon, H.T. (2006). Acetylation of MEK2 and I kappa B kinase (IKK) activation loop residues by YopJ inhibits signaling. Proc. Natl. Acad. Sci. USA *103*, 18574–18579.

Mukhtar, M.S., Deslandes, L., Auriac, M.C., Marco, Y., and Somssich, I.E. (2008). The Arabidopsis transcription factor WRKY27 influences wilt disease symptom development caused by Ralstonia solanacearum. Plant J. *56*, 935–947.

Narusaka, M., Shirasu, K., Noutoshi, Y., Kubo, Y., Shiraishi, T., Iwabuchi, M., and Narusaka, Y. (2009). RRS1 and RPS4 provide a dual Resistance-gene system against fungal and bacterial pathogens. Plant J. *60*, 218–226.

Nicaise, V., Joe, A., Jeong, B.R., Korneli, C., Boutrot, F., Westedt, I., Staiger, D., Alfano, J.R., and Zipfel, C. (2013). Pseudomonas HopU1 modulates plant immune receptor levels by blocking the interaction of their mRNAs with GRP7. EMBO J. *32*, 701–712.

Noutoshi, Y., Ito, T., Seki, M., Nakashita, H., Yoshida, S., Marco, Y., Shirasu, K., and Shinozaki, K. (2005). A single amino acid insertion in the WRKY domain

of the Arabidopsis TIR-NBS-LRR-WRKY-type disease resistance protein SLH1 (sensitive to low humidity 1) causes activation of defense responses and hypersensitive cell death. Plant J. *43*, 873–888.

Ntoukakis, V., Saur, I.M., Conlan, B., and Rathjen, J.P. (2014). The changing of the guard: the Pto/Prf receptor complex of tomato and pathogen recognition. Curr. Opin. Plant Biol. *20*, 69–74.

Oh, H.S., and Collmer, A. (2005). Basal resistance against bacteria in Nicotiana benthamiana leaves is accompanied by reduced vascular staining and suppressed by multiple Pseudomonas syringae type III secretion system effector proteins. Plant J. *44*, 348–359.

Padmanabhan, M.S., Ma, S., Burch-Smith, T.M., Czymmek, K., Huijser, P., and Dinesh-Kumar, S.P. (2013). Novel positive regulatory role for the SPL6 transcription factor in the N TIR-NB-LRR receptor-mediated plant innate immunity. PLoS Pathog. *9*, e1003235.

Rivas, S., and Deslandes, L. (2013). Nuclear components and dynamics during plant innate immunity. Front. Plant Sci. *4*, 481.

Rushton, P.J., Somssich, I.E., Ringler, P., and Shen, Q.J. (2010). WRKY transcription factors. Trends Plant Sci. *15*, 247–258.

Sarris, P.F., Duxbury, Z., Huh, S., Ma, Y., Segonzac, C., Sklenar, J., Derbyshire, P., Cevik, V., Rallapalli, G., Saucet, S.B., et al. (2015). A plant immune receptor detects Pathogen effectors that target WRKY transcription factors. Cell *161*, this issue, 1089–1100.

Sohn, K.H., Hughes, R.K., Piquerez, S.J., Jones, J.D., and Banfield, M.J. (2012). Distinct regions of the Pseudomonas syringae coiled-coil effector AvrRps4 are required for activation of immunity. Proc. Natl. Acad. Sci. USA *109*, 16371–16376.

Sohn, K.H., Segonzac, C., Rallapalli, G., Sarris, P.F., Woo, J.Y., Williams, S.J., Newman, T.E., Paek, K.H., Kobe, B., and Jones, J.D. (2014). The nuclear immune receptor RPS4 is required for RRS1SLH1-dependent constitutive defense activation in Arabidopsis thaliana. PLoS Genet. *10*, e1004655.

Takken, F.L., and Goverse, A. (2012). How to build a pathogen detector: structural basis of NB-LRR function. Curr. Opin. Plant Biol. *15*, 375–384.

Tasset, C., Bernoux, M., Jauneau, A., Pouzet, C., Brière, C., Kieffer-Jacquinod, S., Rivas, S., Marco, Y., and Deslandes, L. (2010). Autoacetylation of the Ralstonia solanacearum effector PopP2 targets a lysine residue essential for RRS1-R-mediated immunity in Arabidopsis. PLoS Pathog. *6*, e1001202.

Thao, S., Chen, C.S., Zhu, H., and Escalante-Semerena, J.C. (2010). Nε-lysine acetylation of a bacterial transcription factor inhibits Its DNA-binding activity. PLoS ONE *5*, e15123.

van der Hoorn, R.A., and Kamoun, S. (2008). From guard to decoy: a new model for perception of plant pathogen effectors. Plant Cell *20*, 2009–2017.

von Moltke, J., Ayres, J.S., Kofoed, E.M., Chavarría-Smith, J., and Vance, R.E. (2013). Recognition of bacteria by inflammasomes. Annu. Rev. Immunol. *31*, 73–106.

Wang, D., Amornsiripanitch, N., and Dong, X. (2006). A genomic approach to identify regulatory nodes in the transcriptional network of systemic acquired resistance in plants. PLoS Pathog. *2*, e123.

Williams, S.J., Sohn, K.H., Wan, L., Bernoux, M., Sarris, P.F., Segonzac, C., Ve, T., Ma, Y., Saucet, S.B., Ericsson, D.J., et al. (2014). Structural basis for assembly and function of a heterodimeric plant immune receptor. Science *344*, 299–303.

Xu, X., Chen, C., Fan, B., and Chen, Z. (2006). Physical and functional interactions between pathogen-induced Arabidopsis WRKY18, WRKY40, and WRKY60 transcription factors. Plant Cell *18*, 1310–1326.

Yamasaki, K., Kigawa, T., Inoue, M., Tateno, M., Yamasaki, T., Yabuki, T., Aoki, M., Seki, E., Matsuda, T., Tomo, Y., et al. (2005). Solution structure of an Arabidopsis WRKY DNA binding domain. Plant Cell *17*, 944–956.

Yamasaki, K., Kigawa, T., Watanabe, S., Inoue, M., Yamasaki, T., Seki, M., Shinozaki, K., and Yokoyama, S. (2012). Structural basis for sequence-specific DNA recognition by an Arabidopsis WRKY transcription factor. J. Biol. Chem. *287*, 7683–7691.

Zhang, H., Li, D., Wang, M., Liu, J., Teng, W., Cheng, B., Huang, Q., Wang, M., Song, W., Dong, S., et al. (2012). The Nicotiana benthamiana mitogen-activated protein kinase cascade and WRKY transcription factor participate in Nep1(Mo)-triggered plant responses. Mol. Plant Microbe Interact. *25*, 1639–1653.

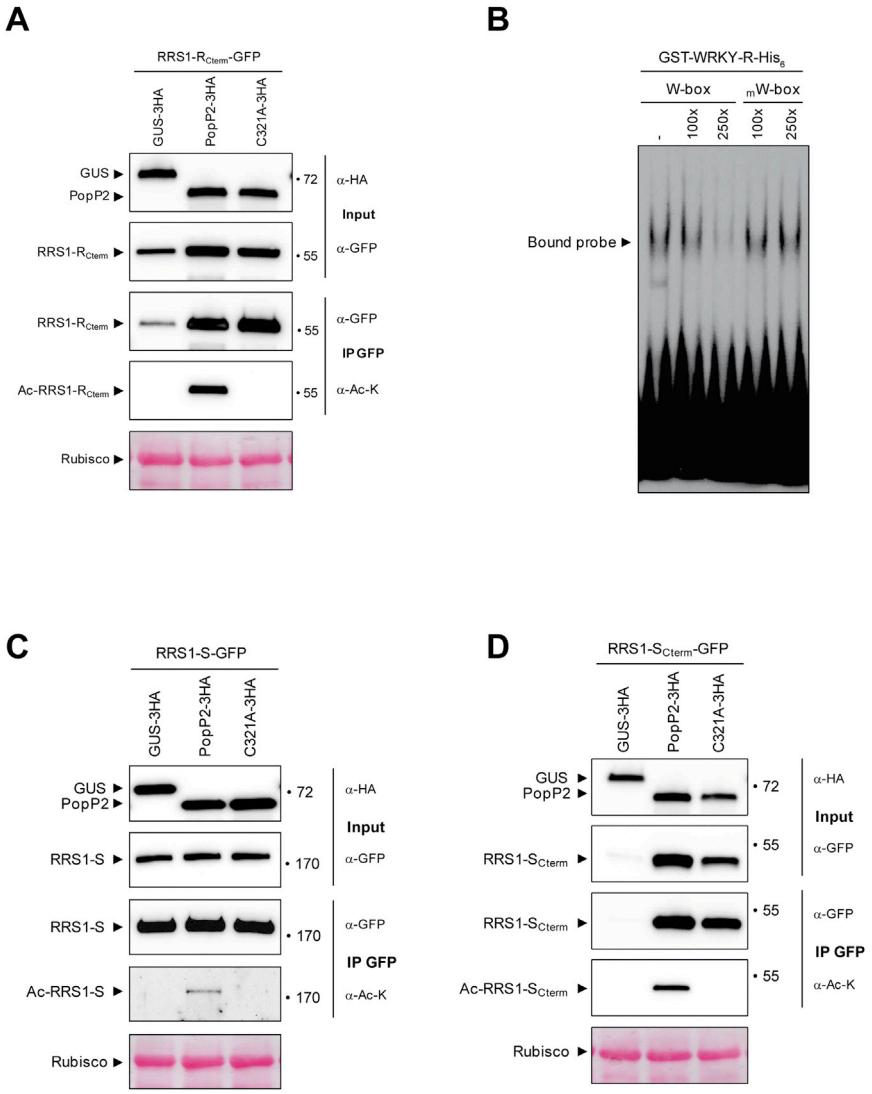

Figure S1. RRS1-R$_{Cterm}$ and RRS1-S$_{Cterm}$ DNA-Binding Domains Are Targeted by PopP2 Acetyltransferase Activity, Related to Figure 1

(A) RRS1-R$_{Cterm}$-GFP was transiently expressed with 3HA-tagged GUS, PopP2 or C321A in *N. benthamiana* leaves. Protein extracts were immunoblotted with anti-GFP (α-GFP) and anti-HA antibodies (α-HA) (Input). IP was performed with anti-GFP beads (IP GFP) and analyzed on immunoblots with α-GFP antibodies for detection of RRS1-R$_{Cterm}$ and with α-acetyl lysine antibodies for detection of acetylated RRS1-R$_{Cterm}$. Results were consistent in three independent experiments. Protein MW: GUS-3HA = 73.5 kDa; PopP2-3HA and C321A-3HA = 58.1 kDa; RRS1-R$_{Cterm}$-GFP = 59.2 kDa.

(B) Gel mobility shift assay of recombinant RRS1-R WRKY domain. The GST-fused protein of the RRS1-R WRKY domain was purified and incubated with labeled W-box and increasing amounts of the unlabeled competitors W-box or mutated W-box (mW-box). Experimental procedures used in this study were similar to (Noutoshi et al., 2005). The W-box and mW-box competitors were added in 100- and 250-fold molar excess. Results were consistent in three independent experiments.

(C and D) PopP2 acetylates RRS1-S WRKY domain. RRS1-S-GFP and RRS1-S$_{Cterm}$-GFP were transiently expressed with 3HA-tagged GUS, PopP2 or C321A in *N. benthamiana* leaves. A similar experimental procedure was carried out as in Figure S1A.

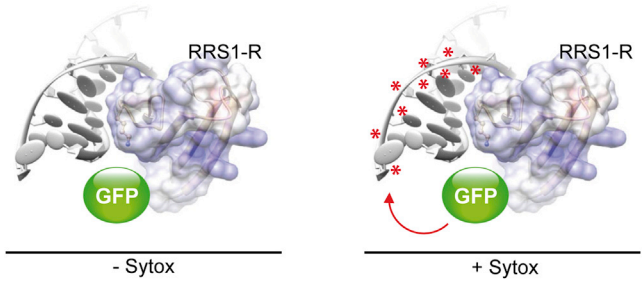

Figure S2. Schematic Representation of FRET-FLIM Measurements for Monitoring Physical Associations between RRS1-R-GFP and DNA, Related to Figure 2

Mean lifetime of GFP fused to RRS1-R (donor) is measured in the absence and in presence of Sytox Orange, a DNA-binding fluorescent dye serving as acceptor (red stars). In the presence of Sytox, a decrease of GFP lifetime indicates a Förster resonance energy transfer (FRET) between donor and acceptor.

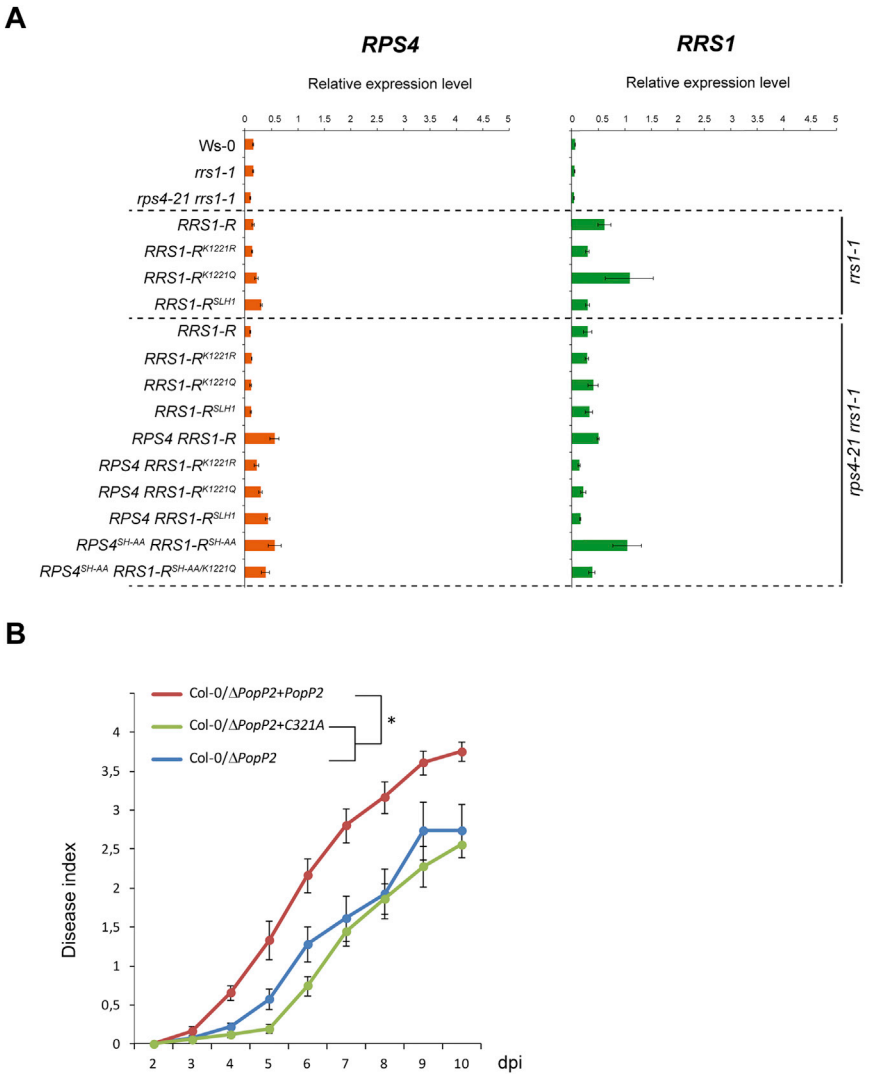

Figure S3. *RPS4* and *RRS1* Expression Levels in Various *Arabidopsis* Lines, Related to Figure 3

(A) *RPS4* and *RRS1* expression level was verified with qRT-PCR using total RNA extracted from 4-week-old plants. Values are means ± SD (n = 9 from three independent transgenic lines in three independent experiments).

(B) PopP2 promotes wilting disease symptom development in *Arabidopsis* Col-0. Individual Col-0 *Arabidopsis* plants were scored from 5 to 10 days after root-inoculation of *R. solanacearum* Δ*PopP2* strain expressing wild-type PopP2 (red line), C321A (green line) or deletant for PopP2 (blue line), using the following scale: 0 = no wilting, 1 = 25%, 2 = 50%, 3 = 75%, and 4 = 100% of wilted leaves (Disease index). Mean and SD values were calculated from scores of a total of 54 plants (from three independent experiments). Covariance analysis (*ANCOVA*) was used to monitor the effect of bacterial strain and time on disease development (http://www.rstudio.org/). Probability (P) values for ANCOVA of the strain/time effect are indicated (*p < 0.05; Student's t test).

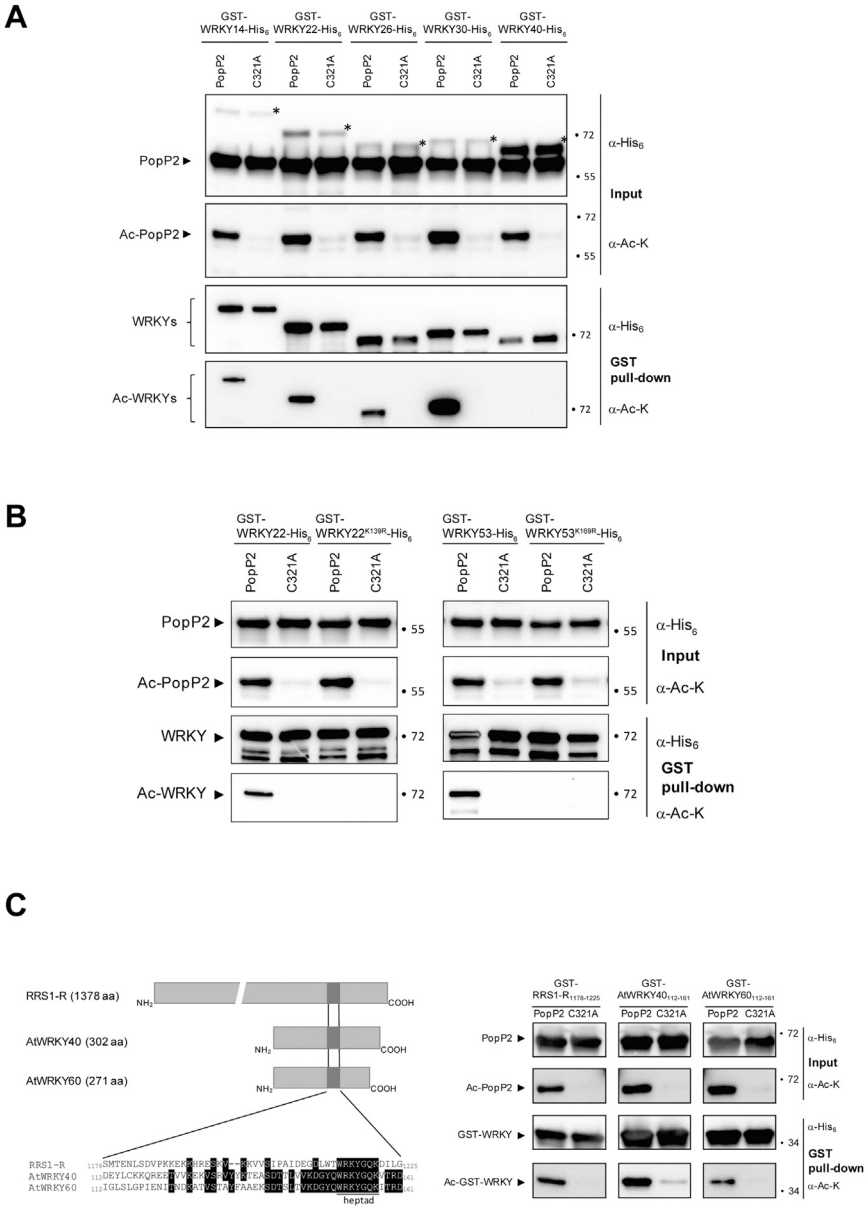

Figure S4. PopP2 Acetylates the Conserved WRKYGQK Heptap of Multiple WRKY Proteins in Bacterial Cells, Related to Figure 4

(A) PopP2 acetylates multiple WRKY proteins in bacterial cells. Recombinant GST-AtWRKY14-His$_6$, GST-AtWRKY22-His$_6$, GST-AtWRKY26-His$_6$, GST-AtWRKY30-His$_6$, and GST-AtWRKY40-His$_6$ were co-expressed either with His$_6$-PopP2 or His$_6$-C321A in *E. coli*. Input indicates protein samples before pull-down (asterisks refer to the expressed GST-fusion proteins). Autoacetylated wild-type PopP2 (Ac-PopP2), but not C321A, is recognized by α-acetyl lysine antibody (Input). Proteins were purified using glutathione sepharose beads and analyzed by immunoblotting using α-His$_6$ and α-acetyl lysine antibodies, as indicated. Results were consistent in at least three independent experiments. Expected protein MW: GST-AtWRKY14-His$_6$ = 79.5 kDa; GST-AtWRKY22-His$_6$ = 65 kDa; GST-AtWRKY26-His$_6$ = 67.7 kDa; GST-AtWRKY30-His$_6$ = 66 kDa; GST-AtWRKY40-His$_6$ = 66.4 kDa; His$_6$-PopP2 and His$_6$-C321A = 55.6 kDa.

(B) PopP2 acetylates the last Lys residue of the conserved WRKY heptad of AtWRKY22 and AtWRKY53. Recombinant GST-AtWRKY22-His$_6$, GST-AtWRKY22^{K139R}-His$_6$, GST-AtWRKY53-His$_6$, and GST-AtWRKY53^{K169R}-His$_6$ were co-expressed either with active His$_6$-PopP2 or catalytically inactive His$_6$-C321A in *E. coli*. A similar experimental procedure was carried out as in Figure S4A. Results were consistent in at least two independent experiments. Expected protein MW: GST-AtWRKY22-His$_6$ = 65 kDa (left); GST-AtWRKY53-His$_6$ = 69 kDa (right).

(C) Truncated domains of RRS1-R, AtWRKY40, and AtWRKY60 containing the conserved heptad WRKY motif (as indicated on the right panel) were fused to GST and co-expressed either with active His$_6$-PopP2 or His$_6$-C321A in *E. coli*. A similar experimental procedure was carried out as in Figure S4A. Results were consistent in at least two independent experiments. Expected protein MW: GST-RRS1-R$_{1178-1225}$-His$_6$ = 38.5 kDa; GST-AtWRKY40$_{112-161}$-His$_6$ = 39 kDa; GST-AtWRKY60$_{112-161}$-His$_6$ = 38.6 kDa.

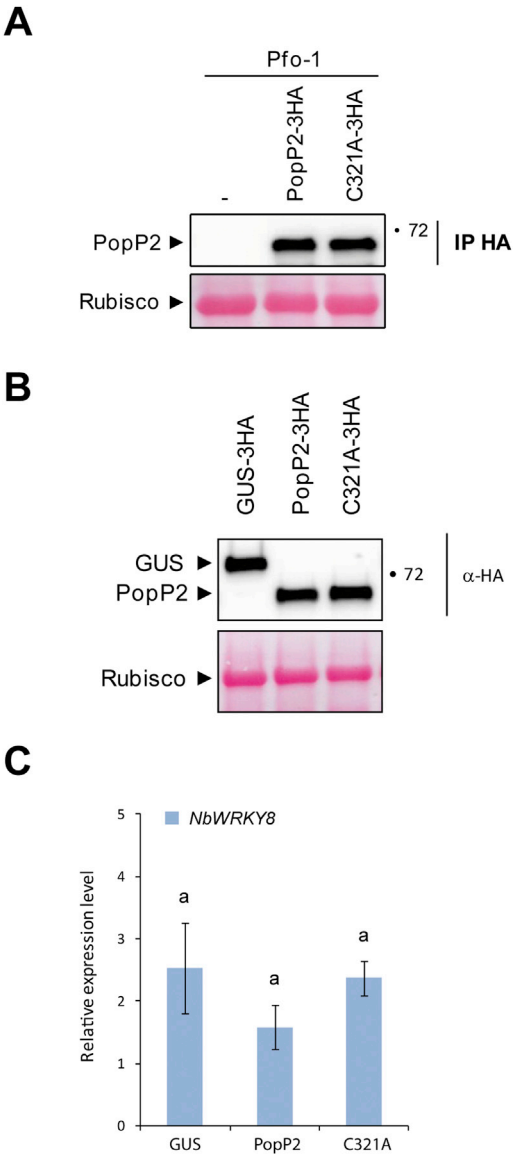

Figure S5. PopP2 Delivered via *Pseudomonas fluorescens* or Expressed via *Agrobacterium* Suppresses PTI Responses, Related to Figure 5

(A) Pfo-1 delivery of PopP2-3HA and C321A-3HA in *N. benthamiana* cells. Accumulation of PopP2 and C321A proteins was confirmed by an IP performed with anti-HA antibodies (IP-HA) followed by immunoblotting with α-HA antibodies. Rubisco is shown as loading control (bottom).

(B) Accumulation levels of GUS, PopP2 and C321A proteins in *N. benthamiana* cells treated with flg22 for PTI inhibition assay. Rubisco is shown as loading control (bottom).

(C) *NbWRKY8* expression is induced at similar levels in flg22-treated *N. benthamiana* cells expressing GUS-3HA, PopP2-HA or C321A-3HA. Expression values represent the mean ± SD from three independent flg22-treated leaf samples relative to water-treated controls. Means labeled with the same letter are not statistically different at the 5% confidence level based on Student's t test.

Cell

Supplemental Information

A Receptor Pair with an Integrated Decoy Converts Pathogen Disabling of Transcription Factors to Immunity

Clémentine Le Roux, Gaëlle Huet, Alain Jauneau, Laurent Camborde, Dominique Trémousaygue, Alexandra Kraut, Binbin Zhou, Marie Levaillant, Hiroaki Adachi, Hirofumi Yoshioka, Sylvain Raffaele, Richard Berthomé, Yohann Couté, Jane E. Parker, and Laurent Deslandes

Supplemental Experimental Procedures

Bacterial Strains and Growth

Escherichia coli DH5 alpha and Rosetta DE3 (Novagen) were grown on Luria broth medium at 37°C. *Pseudomonas fluorescens* (Pfo-1) strain was grown on King's B medium containing chloramphenicol (30 μg/mL) and tetracycline (5 μg/mL) at 28 °C. pBBR1-derived constructs were mobilized to Pfo-1 by triparental mating using *E. coli* HB101 (pRK2013) as a helper strain. Transformed Pfo-1 cells were selected on King's B medium containing chloramphenicol (30 μg/mL), tetracycline (5 μg/mL) and gentamicin (15 μg/mL) at 28 °C. *Agrobacterium tumefaciens* GV3101 cells were transformed with pB7-GWY derived constructs using a standard electroporation method and grown on low-salt LB agar medium containing rifampicin (50 μg/mL), gentamicin (20 μg/mL) and spectinomycin (50 μg/mL) at 28°C. *A. tumefaciens* GV3103 cells transformed with pAM-PAT derived constructs were selected on rifampicin (50 μg/mL), gentamicin (20 μg/mL) and carbenicillin (25 μg/mL) at 28°C.

Plasmid Constructions

Standard DNA cloning methods (Sambrook et al., 1989), PCR, and Gateway technology (Invitrogen) were used for plasmid construction. All primer sequences are listed in Table S2. PCR products flanked by the attB sites were recombined into the pDONR207 vector (Invitrogen) via a BP reaction to create the corresponding entry clones with attL sites (pENTR). pENTR-RRS1-S, pENTR-RRS1-R, pENTR-PopP2, and pENTR-C321A (pDONR207 vector backbone) used in this study have been previously described (Deslandes et al., 2003).

RRS1-R_{Cterm} fragment was amplified from pENTR-RRS1-R by using AttB1-RRS1Cterm and AttB2-RRS1-RCterm primers. *RRS1-*S_{Cterm} fragment was amplified from pENTR-RRS1-S clone by using AttB1-RRS1Cterm and AttB2-RRS1-SCterm primers. *WRKY-R* fragment was amplified from pENTR-RRS1-R by using AttB1-RRS1Cterm and AttB2-RRS1-SCterm. *RPS4 RRS1-R* genomic fragment (11996

bp) containing both *RPS4* and *RRS1-R* genes including 735 bp and 572 bp of RPS4 and RRS1-R terminator sequences respectively, was PCR-amplified from Nd-1 accession by using AttB1-R4T and AttB2-R1T primers, and recombined into pDONR207 to generate pENTR-RPS4-RRS1-R entry clone. RRS1-R genomic fragment (7874 bp) was amplified from Nd-1 by using AttB1-Rprom and Att-R1T primers and recombined into pDONR207 to generate pENTR-RRS1-R genomic entry clone (containing 1000 bp of promoter sequence and 572 bp of terminator).

NbWRKY8 gene was PCR-amplified from *N. benthamiana* genomic DNA by using AttB1-NbWRKY8 and AttB2-NbWRKY8 primers to generate the pENTR-NbWRKY8 entry clone. Appropriate entry clones were subsequently recombined into the following destination vectors via an LR reaction: 1) pCDF-GST-GWY-His_6 (pCDFDuet-1 backbone, Novagen) to create GST-gene-His_6 fusions and pETDuet-1-GWY (pETDuet-1 backbone, Novagen) to create His_6-gene fusions for bacterial acetylation assay; 2) pB7FWG2 for C-terminal fusions to the GFP (gene-GFP) (Karimi et al., 2002); 3) pAM-PAT-GWY-3HA for gene-3HA fusions; 4) pBBR-AvrRps4prom-GWY-3HA for gene-3HA fusions expressed in Pfo-1; 5) pB7FWG2-Δ35S (derived from pB7FWG2 from which 35S promoter sequence has been excised) for *Arabidopsis* transformation (BASTA selection). Donor plasmids containing AtWRKY14, AtWRKY18, AtWRKY22, AtWRKY25, AtWRKY26, AtWRKY27, AtWRKY28, AtWRKY29, AtWRKY30, AtWRKY38, AtWRKY40, AtWRKY41, AtWRKY53, AtWRKY60, and AtWRKY71 open reading frames (pDONR221) were kindly provided by Dr. Imre Somssich. Substitution of the critical "K" residue by an Arginine (R) or a Glutamine (Q) within the coding sequence of the WKRYGQK heptad of various WRKY genes was generated by two-step PCR-based site-directed mutagenesis using PrimeStar HS DNA polymerase from Takara Bio Inc. (Otsu, Japan). The following nucleotide substitutions were done: RRS1-R-K1221R and WRKY-R-K1221R (codon 1221: AAA to AGA), RRS1-R-K1221Q (codon 1221: AAA to CAA), AtWRKY22-K139R (codon 139: AAA to AGA), AtWRKY53-K169R (codon 169: AAA to AGA. Mutations in RPS4 and RRS1-R TIR domains were introduced by using RPS4-TIR-SH-AA-F/RPS4-TIR-SH-AA-R and TIR-R-SH-AA-F/TIR-R-SH-AA-R primers, respectively. All DNA constructs were sequence-verified.

Bacterial Acetylation Assay

Single colonies (*E. coli* Rosetta (DE3) cells (Novagen)) transformed with relative pCDF-GST-gene-His_6 and pETDuet-1-gene destination vectors were grown on LB medium containing carbenicillin (50 µg/mL), spectinomycin (50 µg/mL) and chloramphenicol (30 µg/mL) at 37°C to an OD600nm of 0.6 and induced with 250 µM IPTG (isopropyl-β-thiogalactopyranoside) for 3h at 28 °C. Pelleted cells were concentrated 10 times in PBS [phosphate-buffered saline (pH 8.0)] supplemented with 1 mM phenylmethylsulfonyl fluoride (PMSF, Sigma Aldrich), 10 mM Sodium butyrate, 0.1% Triton, 1mM EDTA, and 2.5 mM DTT) and lysed using a French press. After centrifugation, supernatants were incubated with 30 µL of pre-equilibrated Glutathione Sepharose 4B (GE Healthcare) for 2 h at 4°C with rotation. Sepharose beads were recovered by centrifugation and then washed three times with buffer for 10 min at 4°C with rotation. After denaturation, proteins samples were separated by SDS-PAGE gel (Bio-Rad) and analysed by immunoblot analysis. Transferred proteins were visualized by Ponceau S red staining. Expected protein MW: GST-RRS1-R_{Cterm}-His_6=56.1 kDa, GST-WRKY-R-His_6 = 45.8 kDa; His_6-PopP2 and His_6-C321A= 55.6 kDa.

Immunoprecipitations and Protein Immunoblotting

For immunoprecipitation of fluorescent-tagged proteins, plant protein samples obtained from *N. benthamiana* leaves (4 discs of 8 mm diameter harvested 48 hours post-infiltration) were homogenized in 1mL of ice cold IP Buffer (50 mM Tris HCl pH7.5, 150 mM NaCl, 10 mM EDTA, 2 mM DTT, 5 mM Sodium Butyrate, 1x Plant protease cocktail inhibitor (SIGMA) , 0.1 % Triton). The extract was centrifuged at 13000 g for 2 min at 4°C. 10 µl of GFP-binding protein affinity matrix (Chromotek) was added to the supernatant and rotated at 4°C for 30 min. Samples were centrifuged for 3 min at 1000 g. Beads were washed three times with IP buffer and subsequently boiled in 2 x Laemmli-buffer before analyzing the IPs by immunoblotting (SDS-PAGE). Transferred proteins were visualized by Ponceau S red staining. Membranes were blocked in a 2 % milk TBST (Tris Buffer Saline-Tween 20)

solution before incubation. The following primary antibodies were used in this study: anti-Acetylated Lysine (Ac-K-103, Cell Signaling Technology; dilution 1:2000), anti-HA-HRP (3F10; Roche; dilution 1:5000), anti-GFP (mouse monoclonal; Roche; dilution 1:3000), anti-His_6-HRP (mouse monoclonal; Roche; dilution 1:25000), and anti-all WRKY (rabbit polyclonal; dilution 1:1000 (Turck et al., 2004)). The appropriate horseradish peroxidase-conjugated secondary antibody (Santa Cruz Biotechnology) was applied (goat anti-mouse IgG-HRP or goat anti-rabbit IgG-HRP; dilution 1:10000). Proteins were detected using Clarity Reagent (BioRad). Expected protein MW: GUS-3HA = 73.5 kDa; PopP2-3HA and C321A-3HA = 58.1 kDa; AtWRKY25-GFP = 80 kDa; AtWRKY18-GFP = 70.6 kDa; AtWRKY40-GFP = 69.5 kDa; AtWRKY60-GFP = 66.4 kDa; AtWRKY28-GFP = 71.4 kDa; AtWRKY71-GFP = 67.8 kDa; AtWRKY22-GFP = 68.1 kDa; AtWRKY27-GFP = 74.5 kDa; AtWRKY29-GFP = 69.2 kDa; AtWRKY38-GFP = 69.1 kDa; AtWRKY41-GFP = 70.7 kDa; AtWRKY53-GFP = 72 kDa, RRS1-R-GFP = 184.2 kDa, RRS1-R_{Cterm}-GFP = 51.5 kDa, RRS1-S-GFP = 174 kDa; RRS1-S_{Cterm}-GFP = 41.2 kDa

Mass Spectrometry Analyses

Affinity purified proteins were migrated on an SDS-PAGE gel. After Coomassie blue staining, gel bands were cut out and washed several times by incubation in 25 mM NH_4HCO_3 for 15 min and then in 50 % (v/v) acetonitrile containing 25 mM NH_4HCO_3 for 15 min. In-gel digestion of proteins was realized by overnight incubation at 37°C with 0.15 µg of modified trypsin (Promega, sequencing grade) in 25 mM NH_4HCO_3. Peptides were then extracted from gel pieces in three 15 min sequential extraction steps in 30 µL of 50% acetonitrile, 30 µL of 5% formic acid and finally 30 µL of 100% acetonitrile. The pooled supernatants were then dried under vacuum. For nano-LC-MS/MS analysis, the dried extracted peptides were resuspended in 30 µl of water containing 2.5 % acetonitrile and 0.1 fluoroacetic acid. Classical nanoLC-MS analyses were performed using reverse-phase fractionation of peptides with an Ultimate 3000 system (Dionex) and MS/MS analyses using a LTQ-Orbitrap Velos (Thermo Scientific). Raw MS data were acquired using Xcalibur (Thermo Scientific) and automatically processed through Mascot Daemon software (version 2.3.2, Matrix Science).

Concomitant searches of the UniProt protein databank (*Nicotiana benthamiana* taxonomy), classical contaminant protein sequence databases, tested recombinant proteins sequences, and the corresponding reversed databases were performed using Mascot (version 2.4). The following peptide modifications were allowed during the search: carbamidomethyl (C, fixed), acetyl (N-ter, variable), oxidation (M, variable) and acetylation (K, variable). The IRMa software (version 1.31.1) (Dupierris et al., 2009) was used to filter out the results by only conservation of rank 1 peptides and of peptides exhibiting query homology threshold with p-value inferior to 0.01.

FRET-FLIM Measurements

Fluorescence lifetime measurements were performed in time domain using a streak camera. The light source is a mode-locked Ti:sapphire laser (Tsunami, model 3941, Spectra-Physics, USA) pumped by a 10W diode laser (Millennia Pro, Spectra-Physics) and delivering ultrafast femtosecond pulses of light with a fundamental frequency of 80MHz. A pulse picker (model 3980, Spectra-Physics) is used to reduce the repetition rate to 2MHz to satisfy the requirements of the triggering unit (working at 2MHz). The experiments were carried out at λ = 860 nm (multiphoton excitation mode). All images were acquired with a 60x oil immersion lens (plan APO 1.4 N.A., IR) mounted on an inverted microscope (Eclipse TE2000E, Nikon, Japan). The fluorescence emission is directed back into the detection unit through a short pass filter λ<750 nm) and a band pass filter (515/30 nm). The detector is a streak camera (Streakscope C4334, Hamamatsu Photonics, Japan) coupled to a fast and high-sensitivity CCD camera (model C8800-53C, Hamamatsu). For each nucleus, average fluorescence decay profiles were plotted and lifetimes were estimated by fitting data with exponential function using a non-linear least-squares estimation procedure. Fluorescence lifetime of the donor (GFP) was experimentally measured in the presence and absence of the acceptor (Sytox Orange). FRET efficiency (E) was calculated by comparing the lifetime of the donor in the presence (τ_{DA}) or absence (τ_D) of the acceptor: $E=1-(\tau_{DA}) / (\tau_D)$. Statistical comparisons between control (donor) and assay

(donor + acceptor) lifetime values were performed by Student's t-test. For each experiment, eight leaf discs removed from four *A. tumefaciens* infiltrated leaves were used to collect data.

EMSA

The coding sequence corresponding to the WRKY domain of RRS1-R (residues 1190 to 1290 of RRS1-R) was cloned into pCDF-GST-GWY-His_6 destination vector to create pCDF-GST-WRKY-R-His_6 expression vector. Nonacetylated and acetylated GST-WRKY-R-His_6 proteins were produced following instructions described in the Bacterial acetylation assay procedure. GST affinity purified proteins were eluted in elution buffer (40 mM reduced Glutathione pH=8.0) and adjusted to 10% glycerol. Five to 10 micrograms of purified GST–WRKY-R-His_6 fusion protein were incubated with biotin labelled W-box DNA probe in binding reaction buffer (LightShift Chemiluminsecent EMSA kit, Pierce) at room temperature for 20 min. Binding reactions were separated on a 6% polyacrylamide gel and transferred to a Nylon membrane. Crossed-linked membranes were subjected to the detection of biotin-labeled DNA by chemiluminescence according to manufacturer's instructions. Competition assays with unlabelled W-box and mutated W-box were performed as previously described (Noutoshi et al., 2005).

WRKY Domain Modeling

The model of RRS1 WRKY domain (residues 1192 to 1273) bound to DNA was built using Modeller9v12 (Eswar et al., 2006) with models 2LEX and 2AYD as templates. The model of RRS1Kac1221 was built using Modeller 'automodel' function with RRS1 and acetylated lysine models as templates. RRS1 K1221Q, K1221R and SLH1 variant models were built using modeller 'mutate' function. For each structure, five models were obtained by modeller and the best one was selected using DOPE and GA341 assess methods in Modeller as well as Procheck analysis. Electrostatic potentials were calculated through PDB2PQR server (Dolinsky et al., 2004) using CHARMM forcefield,

and the Adaptive Poisson-Boltzmann Software (APBS) (Baker et al., 2001). Image color spectra were analyzed with ImageJ 1.47.

Plant Materials, Growth Conditions, and Pathology Assays

Arabidopsis Col-0 plants were grown in Jiffy pots under controlled conditions (22°C, 60% relative humidity, 125 µE/M2/s fluorescent illumination, 8 h light:16 h dark cycle.). Inoculations with *Ralstonia solanacearum* cells (*Rs*∆*PopP2*, *Rs*∆*PopP2* PopP2-3HA and *Rs*∆*PopP2* C321A-3HA; OD600=0.01) were performed on four-week old Arabidopsis plants as described (Deslandes et al., 1998). A covariance analysis was used to monitor the effect of each bacterial strain on disease development as described.

RNA Isolation and Quantitative RT-PCR

Material for RNA analysis was ground in liquid nitrogen, and total RNA was isolated using the Nucleospin RNA plant kit (Macherey-Nagel) according to the manufacturer's recommendations. 1 µg of RNA was used for cDNA synthesis. Real-time quantitative PCR was performed on a Light Cycler 480 II machine (Roche Diagnostics) using Roche reagents. For *N. benthamiana*-related assays, *NbEF1-*α expression was used to normalize the expression value in each sample and relative expression values were determined against the average value of control corresponding to sample expressing either GUS, PopP2 or C321A using the comparative Ct method ($2^{\Delta Ct}$) (Livak, 1997 & 2001). Average ∆Ct was calculated from three independent biological replicates (2 leaves/2 plants). For *A. thaliana*-related assays, relative expression values were determined against the average value of samples expressing RPS4-RRS1 derived constructs using the comparative Ct method ($2^{\Delta Ct}$). Average ∆Ct was calculated from three technical replicates and three independent biological replicates corresponding to three independent *rrs1-1* or *rps4-21 rrs1-1* mutant lines complemented with relative genomic constructs. Expression values were normalized using average value of *AtEF1-*

α. Significance of the results was assessed using a two-tailed *t*-test. Primers used for qRT-PCR analysis are listed in Supplemental Table S2.

PTI Inhibition Assays

PopP2 allelic sequences were introduced by LR recombination in pBBR1-AvrRps4prom-GWY-3HA destination vector that allows the expression, under the control of AvrRps4 promoter sequence (504 bp of promoter sequence PCR-amplified from *avrRps4*^{Pip151} genomic clone), of proteins tagged in the C-terminus end with 3-HA epitope tag. To confirm the expression of PopP2 variants delivered by Pfo-1 (Thomas et al., 2009), 4 leaf discs of *N. benthamiana* were harvested 7 h after infiltration with bacterial suspensions (OD600nm = 0.2 in 10 mM MgCl2). IPs of 3HA-tagged proteins were performed using anti-HA affinity matrix (Roche) according to the procedure described for purification of GFP-tagged proteins (see Immunoprecipitation and protein immunoblotting). For suppression of PTI elicited by Pfo-1 in *N. benthamiana* (Figure 5) bacterial suspensions of Pfo-1, Pfo-1 PopP2, Pfo-1 C321A at OD600nm = 0.2 in 10 mM MgCl2 were infiltrated into fully expanded leaves of *N. benthamiana*. PTI was allowed to develop during 7 h, after which a *P. syringae* pv. *tomato* DC3000 suspension at OD600 = 0.02 was infiltrated into an overlapping area. Tissue collapse in the overlapping area was evaluated at 2 days post infiltration.

N. benthamiana leaf discs expressing GUS-3HA, PopP2-3HA or C321A-3HA were collected 24 h post-agroinfiltration and soaked overnight in water. Samples were then treated with 100 nM flg22 or distilled water for 45 min. mRNAs were extracted from treated leaf discs and qRT-PCR was conducted to determine the expression of *NbGRAS2*, *NbACRE132* and *NbPti5* genes in flg22-treated leaf discs relative to water-treated leaf discs. All samples were normalized against the reference gene *NbEF1*α. The same material was used to monitor the expression level of *NbWRKY8*, *NADP-ME*, *HMGR2* and *NbACS2* genes.

Table S2. Primers Used in This Study, Related to the Supplemental Experimental Procedures

Primer name	Sequence
AttB1-R4T	GGGGACAAGTTTGTACAAAAAAGCAGGCTTATCAAATGTACTAGACTTTGG
AttB2-R1T	GGGGACCACTTTGTACAAGAAAGCTGGGTCATTTTAGGTAATTTTCATATACT
AttB1-Rprom	GGGGACAAGTTTGTACAAAAAAGCAGGCTTATTACCTAAAGCACCCACGA
TIR-R-SH-AA-F	GTACTCTTTCGTGGCAGCTCTCTCTGAAGCTCTCCGTCGAAAAGGCAT
TIR-R-SH-AA-R	GAGAGCTTCAGAGAGAGCTGCCACGAAAGAGTACCGTACCTCTTCTA
RPS4-TIR-SH-AA-F	TGCGCCGGAGATTCGTCGCAGCTCTCGTCACGGCCTTGAAATT
RPS4-TIR-SH-AA-R	AAGGCCGTGACGAGAGCTGCGACGAATCTCCGGCGCAAATCT
AttB1-RRS1Cterm	GGGGACAAGTTTGTACAAAAAAGCAGGCTTAATGGGTTTCGATATATGTTATA
AttB2-RRS1-SCterm	GGGGACCACTTTGTACAAGAAAGCTGGGTCGCAGATGGAGGAGGAAGT
AttB2-RRS1-RCterm	GGGGACCACTTTGTACAAGAAAGCTGGGTCAAAGTAAAAATTATAATCATCGAA
RRS1-R-K1221R-F	GACTTGGCGAAAGTACGGTCAAAGAGACATCTTA
RRS1-R-K1221R-R	TCTTTGACCGTACTTTCGCCAAGTCCATAGATCTCC
RRS1-R-K1221Q-F	GACTTGGCGAAAGTACGGTCAACAAGACATCTTA
RRS1-R-K1221Q-R	TTGTTGACCGTACTTTCGCCAAGTCCATAGATCTCC
slh1-rev	GAAAACGAGAACCTAATAAGATGTCTTTTTGACCGT
slh1-Fw	AAAAGACATCTTATTAGGTTCTCGTTTTCCAAGGGGT
AttB1-RRS1-R	GGGGACAAGTTTGTACAAAAAAGCAGGCTTGATGACCAATTGTGAAAAGGAT
AttB2-RRS1-R	GGGGACCACTTTGTACAAGAAAGCTGGGTCAAAGTAAAAATTATAATCATCGAA
AttB1-AtWRKY22	GGGGACAAGTTTGTACAAAAAAGCAGGCTTAATGGCCGACGATTGGGA
AttB2-AtWRKY22	GGGGACCACTTTGTACAAGAAAGCTGGGTCTATTCCTCCGGTGGTAGT
AtWRKY22-Fw	ATGGCCGACGATTGGGATCTCCACGCCGTAGTCA
AtWRKY22-K139R-Rev	ACCTTTGATGGGTCTCTGTCCGTACTTTCGCCATGCCCA
AtWRKY22-K139R-Fw	AGTACGGACAGAGACCCATCAAAGGTTCACCATATCCA
AtWRKY22-Rev	TATTCCTCCGGTGGTAGTGGCGGCACTGTTCACAA
AttB1-AtWRKY53	GGGGACAAGTTTGTACAAAAAAGCAGGCTTAATGGAAGGAAGAGATATGTT
AttB2-AtWRKY53	GGGGACCACTTTGTACAAGAAAGCTGGGTCATAATAAATCGACTCGTGTAA
AtWRKY53-Fw	ATGGAAGGAAGAGATATGTTAAGTTGGGAGCAAAAGA
AtWRKY53-K169R-Rev	GCCTAAAATGTCTCTTTGACCATATTTTCTCCAGCTAAAGA
AtWRKY53-K169R-Fw	AAATATGGTCAAAGAGACATTTTAGGCGCCAAATTCCCA
AtWRKY53-Rev	ATAATAAATCGACTCGTGTAAAAACGCGGGGAAAGT
AttB1-R-1178-1225	GGGGACAAGTTTGTACAAAAAAGCAGGCTTAATGTCCATGACCGAGAATTTGTCTGACGT
AttB2-R-1178-1225	GGGGACCACTTTGTACAAGAAAGCTGGGTCACCTAAGATGTCTTTTTGAC
AttB1-W40-112-161	GGGGACAAGTTTGTACAAAAAAGCAGGCTCCATGGATGAGTATTTGTGTAAGAAG
AttB2-W40-112-161	GGGGACCACTTTGTACAAGAAAGCTGGGTCATTGTCTCTAGTCACTTTCTGT
AttB1-W60-112-161	GGGGACAAGTTTGTACAAAAAAGCAGGCTTAATGATTGGACTCAGTCTCGGA
AttB2-W60-112-161	GGGGACCACTTTGTACAAGAAAGCTGGGTCATTATCTCTCGTAATCTTTTGCC
PR2-F (At3g57260)	GCTTAGCCTCACCACCAATG
PR2-R (At3g57260)	CCCGTAGCATACTCCGATTT
PR5-F (At1g75040)	CGGACTACTCGAGGATTTTCA
PR5-R (At1g75040)	GTGCTCGTTTCGTCGTCATA
SAG13-F (At2g29350)	AGGAAAACTCAACATCCTCGTC
SAG13-R (At2g29350)	GCTGACTCGAGATTTGTAGCC
AtEF-1 Fwd	TGTGGAAGTTTGAGACCACC
AtEF-1 Rev	GCAAGCAATGCGTGCTCAC
AttB1-NbWRKY8	GGGGACAAGTTTGTACAAAAAAGCAGGCTTAATGGCAGCTTCTTCAACAAT
AttB2-NbWRKY8	GGGGACCACTTTGTACAAGAAAGCTGGGTCGCAGAGCAATGTCTCCATA
HMGR2-Fw	CCAGGGATAACAATGATGATTC
HMGR2-Rv	CAGCCAAGCGTAGTTGCG
NADP-ME	GTCTTCCTCTGTCACCTGACC
NADP-ME	AAACATTTACGAAGGAAGTCGTG

NbACS2-Fw	TGATTGTCAAGAGCCAGG
NbACS2-Rv	TGGTGAGTGAGGGATAGGAGATG
NbPti5-F	CCTCCAAGTTTGAGCTCGGATAGT
NbPti5-R	CCAAGAAATTCTCCATGCACTCTGTC
NbGRAS2-F	TACCTAGCACCAAGCAGATGCAGA
NbGRAS2-R	TCATGAGGCGTTACTCGGAGCATT
NbACRE132-F	AAGGTCCAGCGAAGTCTCTGAGGGTGA
NbACRE132-R	AAGAATTCCAATCCTAGCTCTGGCTCCTG
NbEF1a-F	AAGGTCCAGTATGCCTGGGTGCTTGAC
NbEF1a-R	AAGAATTCACAGGGACAGTTCCAATACCAC
RPS4-Fw	CGGCTGCTCAACTTTTAAGG
RPS4-rev	GGCCTGGAATTTCCTCTAGC
RRS1-Fw	TGATAGGTTCACAGTGAGAA
RRS1-rev	TGGTACGTCAGACAAATTC

Supplemental References

Baker, N.A., Sept, D., Joseph, S., Holst, M.J., and McCammon, J.A. (2001). Electrostatics of nanosystems: application to microtubules and the ribosome. Proc Natl Acad Sci U S A *98*, 10037-10041.

Deslandes, L., Olivier, J., Peeters, N., Feng, D.X., Khounlotham, M., Boucher, C., Somssich, I., Genin, S., and Marco, Y. (2003). Physical interaction between RRS1-R, a protein conferring resistance to bacterial wilt, and PopP2, a type III effector targeted to the plant nucleus. Proc Natl Acad Sci U S A *100*, 8024-8029.

Deslandes, L., Pileur, F., Liaubet, L., Camut, S., Can, C., Williams, K., Holub, E., Beynon, J., Arlat, M., and Marco, Y. (1998). Genetic characterization of RRS1, a recessive locus in Arabidopsis thaliana that confers resistance to the bacterial soilborne pathogen Ralstonia solanacearum. Mol Plant Microbe Interact *11*, 659-667.

Dolinsky, T.J., Nielsen, J.E., McCammon, J.A., and Baker, N.A. (2004). PDB2PQR: an automated pipeline for the setup of Poisson-Boltzmann electrostatics calculations. Nucleic Acids Res *32*, W665-667.

Dupierris, V., Masselon, C., Court, M., Kieffer-Jaquinod, S., and Bruley, C. (2009). A toolbox for validation of mass spectrometry peptides identification and generation of database: IRMa. Bioinformatics *25*, 1980-1981.

Eswar, N., Webb, B., Marti-Renom, M.A., Madhusudhan, M.S., Eramian, D., Shen, M.Y., Pieper, U., and Sali, A. (2006). Comparative protein structure modeling using Modeller. Curr Protoc Bioinformatics *Chapter 5*, Unit 5.6.

Karimi, M., Inzé, D., and Depicker, A. (2002). GATEWAY vectors for Agrobacterium-mediated plant transformation. Trends Plant Sci *7*, 193-195.

Livak, K.J. (1997 & 2001). ABI Prism 7700 Sequence detection System User Bulletin #2. Relative quantification of gene expression. ABI company publication.

Noutoshi, Y., Ito, T., Seki, M., Nakashita, H., Yoshida, S., Marco, Y., Shirasu, K., and Shinozaki, K. (2005). A single amino acid insertion in the WRKY domain of the Arabidopsis TIR-NBS-LRR-WRKY-type disease resistance protein SLH1 (sensitive to low humidity 1) causes activation of defense responses and hypersensitive cell death. Plant J *43*, 873-888.

Sambrook, J., Fritsch, E., and Maniatis, T. (1989). Molecular cloning: A laboratory manual. Cold Spring Harbor: Cold Spring Harbor Laboratory Press.

Thomas, W.J., Thireault, C.A., Kimbrel, J.A., and Chang, J.H. (2009). Recombineering and stable integration of the Pseudomonas syringae pv. syringae 61 hrp/hrc cluster into the genome of the soil bacterium Pseudomonas fluorescens Pf0-1. Plant J *60*, 919-928.

Turck, F., Zhou, A., and Somssich, I.E. (2004). Stimulus-dependent, promoter-specific binding of transcription factor WRKY1 to Its native promoter and the defense-related gene PcPR1-1 in Parsley. Plant Cell *16*, 2573-2585.